also associated with LOAD.[4,5] Although this association has noted contradictory results,[6] a clearance pathway of β-amyloid could link to cholesterol metabolism.[7]

In contrast, epidemiological studies have indicated that statins could protect against the occurrence of dementia including AD,[8] and cholesterol metabolism has been identified as a prevention target. Indeed, in patients with LOAD, the ratio of HDL to LDL cholesterol significantly decreased by the *APOE-ε4* dose, suggesting that lipid metabolism could be altered in patients with LOAD.[9] Cholesterol metabolism in the brain occurs in a highly closed environment compared to other organs such as the liver and muscles.[10] It is assumed that 24S-hydroxycholesterol is the transport form for cholesterol across the blood–brain barrier,[11] and it has been proposed that the gene encoding cholesterol 24S-hydroxylase (CYP46) is associated with the occurrence of AD, brain β-amyloid load, and phosphorylated tau.[12,13]

In contrast to cholesterol, fatty acid delivery could have direct significance in respect to the supply of essential polyunsaturated fatty acids in the brain, because fatty acids can be selectively transported into the brain across the blood–brain barrier.[14] However, the concentration of free fatty acids in serum and cerebrospinal fluid could modify the fatty acid environment in the brain. Albumin, the major protein in plasma, shows high affinity with free fatty acids,[15] and it was noted that a large majority (~89%) of β-amyloid is bound to albumin.[16] Since albumin exists not only in plasma but also in cerebrospinal fluid, it could also play a role in the delivery of β-amyloid between the brain and the systemic circulation. Therefore, we examined the association of the *ALB* gene with the occurrence of LOAD using a microsatellite polymorphism located in intron 4. We show herein that the *ALB* gene is associated with the occurrence of LOAD in elderly Japanese subjects.

SUBJECTS AND METHODS

Subjects

Probable AD ($n = 224$) and definite AD ($n = 61$) were diagnosed according to the criteria of the National Institute of Neurological and Communicative Disorders and Stroke – Alzheimer's Disease and Related Disorders Association.[17] Non-demented control subjects were obtained from the spouses of the patients ($n = 30$), outpatients ($n = 242$), and healthy volunteers ($n = 384$). Genomic DNA samples were obtained from the blood leukocytes of subjects with written informed consent, according to the procedure approved by the Genome Ethical Committee in Osaka University Graduate School of Medicine, Ehime University School of Medicine, and Fukushimura Hospital, Japan. The age at onset, for stage 3 of the Functional Assessment of Staging (FAST), was determined based on an interview with a knowledgeable informant and a review of the medical records. The mean ± SD age at blood drawing of the patients ($n = 285$) was 78.3 ± 8.18 years (range 60–97 years), and that of the controls ($n = 656$) was 76.1 ± 6.11 years (range 61–90 years). The mean ± SD age at onset was 72.6 ± 7.69 years (range 60–90 years).

Genotyping

To amplify the microsatellite located in intron 4, genomic DNA was amplified using primers ALB1: ATTGATTTCGTTTTAGTCAGCAAC, and ALB2: TGATGGTCTTGTCTCTGTCATTC, under the standard reaction conditions (Applied Biosystems, Foster City, CA, USA). To amplify the microsatellite located in intron 11, primers ALB3: CAAAAAGAATGC CCTGTGC and ALB4: CCTGGACAACAAAGC GAGAC were used. Both polymerase chain reactions (PCR) were performed at 94°C for 30 s, 55°C for 30 s, and 72°C for 30 s for 40 cycles. The length variation of these microsatellites was examined by electrophoresis in 3% agarose gel. PCR amplification of 10 different DNA samples indicated that the intron 4 microsatellite was polymorphic, but the intron 11 microsatellite was not. Therefore, the intron 4 microsatellite was further genotyped as a polymorphic marker of the *ALB* gene by PCR reaction using carboxyl-fluorescein (FAM)-labeled ALB1 and non-labeled ALB2, followed by length measurement using a capillary sequencer, MegaBACE 1000 (Amersham, Piscataway, NJ, USA).

Statistics

The allele distribution between LOAD and control groups were compared by $2 \times n$ χ^2 statistics, where a cell containing the number of less than 5 was combined with its neighboring cell. The allele and genotype frequencies were tested by 2×2 χ^2 statistics. To test whether the effect of dose of the allele with 11 CA repeat, termed $(CA)_{11}$ allele, was independent of the *APOE-ε4* dose, logistic regression of the occurrence of LOAD was performed with the *APOE-ε4* dose and age at blood drawing. Age at onset was in regular distribution by Kolmogorov-Smirnov test ($P = 0.11$), and the correlation between age at onset and the dose of the $(CA)_{11}$ allele, assuming codominant effect, was examined by regression analysis. *P*-values less than 0.05 were considered significant.

Table 1. Allele frequencies of the intron 4 microsatellite

(CA)n allele	LOAD ($n = 570$)*	Control ($n = 1312$)
9	2 [0.004]	2 [0.002]
10	0 [0]	2 [0.002]
11	419 [0.735]	1042 [0.794]†
12	24 [0.042]	38 [0.029]
13	109 [0.191]	208 [0.159]
14	14 [0.025]	19 [0.014]
15	0 [0]	0 [0]
16	0 [0]	1 [0.001]
17	2 [0.004]	0 [0]

*The data was analyzed by 2×9 χ^2 statistics. The allele distribution was significantly different between LOAD and control groups ($P < 0.05$).

†The data was analyzed by 2×2 χ^2 statistics. The $(CA)_{11}$ allele occurred at a significantly higher frequency in the control group than in the LOAD group ($P < 0.005$).

Table 2. Genotype frequencies of the intron 4 microsatellite

(CA)n genotype	LOAD ($n = 285$)	Control ($n = 656$)
9/11	2 [0.007]	2 [0.003]
10/11	0 [0.000]	2 [0.003]
11/11	156 [0.547]	409 [0.623]
11/12	10 [0.035]	28 [0.043]
11/13	85 [0.298]	174 [0.265]
11/14	10 [0.035]	17 [0.026]
11/16	0 [0.000]	1 [0.002]
12/12	4 [0.014]	2 [0.003]
12/13	4 [0.014]	6 [0.009]
12/14	2 [0.007]	0 [0.000]
13/13	9 [0.032]	13 [0.020]
13/14	2 [0.007]	2 [0.003]
17/17	1 [0.004]	0 [0.000]

RESULTS

Association of the intron 4 microsatellite

The number of CA repeats in this microsatellite ranged from 9 to 17, and the $(CA)_{11}$ allele was the most frequent both in LOAD and control groups (Table 1). The allele distribution was significantly different between the groups ($P < 0.05$), and the $(CA)_{11}$ allele occurred at a significantly higher frequency in control group than in LOAD group ($P < 0.005$). The genotype frequency of the intron 4 microsatellite was in Hardy–Weinberg equilibrium in both LOAD and control groups (Table 2). The genotype homozygous for the $(CA)_{11}$ allele was the most frequent in both groups, and the genotype distribution was not significantly different. Nonetheless, the $(CA)_{11}/(CA)_{11}$ genotype was more frequent in LOAD than in control subjects, reflecting the difference of allele distribution. Therefore, we examined further the $(CA)_{11}$ allele.

Table 3. Odds ratio of the $(CA)_{11}$ allele: Odds ratio stratified by genotypes

Genotype	LOAD ($n = 285$)	Control ($n = 656$)	Odds ratio [95% CI]
–\–	22	23	1.0 [Reference]
$(CA)_{11}$/–	107	224	0.49 [0.27–0.94]*
$(CA)_{11}/(CA)_{11}$	156	409	0.40 [0.22–0.74]**
$(CA)_{11}$+	263	633	0.43 [0.24–0.79]***

*$P < 0.05$; **$P < 0.005$; ***$P < 0.01$.

$(CA)_{11}$ means allele of the intron 4 microsatellite harboring 11 CA repeat.

–/–, $(CA)_{11}$ non-carrier; $(CA)_{11}$/–, $(CA)_{11}$ hetero carrier; $(CA)_{11}/(CA)_{11}$, $(CA)_{11}$ homo carrier; $(CA)_{11}$+, all $(CA)_{11}$ carrier.

Table 4. Odds ratio of the $(CA)_{11}$ allele: Logistic regression in codominant model

Variables	Estimated odds ratio	95% CI	*P*-value
Age	1.05	[1.03–1.07]	<0.0001
APOE-ε4	3.96	[2.98–5.26]	<0.0001
$(CA)_{11}$ allele	0.70	[0.54–0.90]	<0.005

$(CA)_{11}$ means allele of the intron 4 microsatellite harboring 11 CA repeat.

Odds ratio in the $(CA)_{11}$ allele

When the alleles were divided into the $(CA)_{11}$ and the other alleles, subjects carrying the $(CA)_{11}$ allele significantly showed a reduced risk for LOAD compared to non-carriers (OR = 0.43, 95% CI = 0.24–0.79, $P < 0.01$), and this reduced risk was more prominent in $(CA)_{11}/(CA)_{11}$ subjects (OR = 0.40, 95% CI = 0.22–0.74, $P < 0.005$) (Table 3). We tested whether the effect of the $(CA)_{11}$ allele was independent of age and the *APOE-ε4* dose. Logistic regression under codominant effect of the $(CA)_{11}$ allele indicated that the $(CA)_{11}$ allele was protective against LOAD independently of age and the *APOE-ε4* dose (OR = 0.70, 95% CI = 0.54–0.90, $P < 0.005$) (Table 4).

Age differences in genotype and allele distribution

We examined whether the allele distribution differed by age. When subjects were stratified into 10-year

Table 5. Age comparisons of the intron 4 microsatellite genotypes and alleles

Age of subject	Genotype $(CA)_{11}/(CA)_{11}$	$(CA)_{11}/-$	$-/-$	Allele $(CA)_{11}$
Load				
60–69	27 [0.551]	16 [0.327]	6 [0.122]	70 [0.714]
70–79	61 [0.555]	40 [0.364]	9 [0.082]	162 [0.736]
80–89	56 [0.533]	42 [0.400]	7 [0.067]	154 [0.733]
90–	12 [0.571]	9 [0.429]	0 [0.000]	33 [0.786]
Control				
60–69	43 [0.642]	22 [0.328]	2 [0.030]	108 [0.806]
70–79	254 [0.624]	137 [0.332]	16 [0.039]	645 [0.792]
80–89	107 [0.611]	63 [0.360]	5 [0.029]	277 [0.791]
90–	5 [0.714]	2 [0.286]	0 [0.000]	12 [0.857]

$(CA)_{11}/(CA)_{11}$, $(CA)_{11}$ homo carrier; $(CA)_{11}/-$, $(CA)_{11}$ hetero carrier; $-/-$, $(CA)_{11}$ non-carrier.

intervals by age at blood drawing, the genotype frequency in the control subjects was similar. The age group equal to and older than 90 years old showed an increased frequency of the $(CA)_{11}/(CA)_{11}$ genotype, but this trend was not significant (Table 5). Subjects with LOAD showed the same trend as control subjects. In contrast, the $(CA)_{11}/(CA)_{11}$ genotype in the control subjects was higher than that in LOAD subjects in all age groups. Therefore, the protective effect of the $(CA)_{11}$ allele for LOAD was not likely related to age. Regression analysis also did not support any effect of the $(CA)_{11}$ allele for age at onset.

DISCUSSION

We showed that the intron 4 microsatellite of the *ALB* gene was polymorphic, that the $(CA)_{11}$ allele was significantly over-represented in non-demented controls more than LOAD. This deviation could be attributable to single nucleotide polymorphisms in linkage disequilibrium with the intron 4 microsatellite, because it was noted that more than 20 different mutations of the *ALB* gene have been reported.[16] Therefore, a detailed evaluation of the sequence variation in the *ALB* gene is warranted in respect of LOAD, along with a confirmation in different ethnic backgrounds. In contrast, intronic microsatellite sequence in itself, could alter the splicing efficiency and transcription factor binding, but this possibility should be examined by splicing and transcription assays.

While albumin is a major transporter of β-amyloid, the etiological relationship of albumin with LOAD could be complicated because of its ubiquitous localization and multifunctional properties. Albumin is mainly synthesized in the liver and secreted into blood, and comprises about half of all serum protein. Albumin binds and transports long-chain fatty acids, binds and detoxificates unconjugated bilirubin, plays a secondary or backup role in the transport of thyroid and steroid hormones, and stabilizes extracellular fluid volume by maintaining osmotic pressure. Albumin also binds and transports metals such as zinc, calcium and magnesium, and the serum albumin level had been utilized as an indicator of nutritional status regarding proteins, and, to some extent, the functional reserve of the liver.[18] Albumin is also the most abundant protein in cerebrospinal fluid, mainly secreted from the choroid plexuses. Only a small percentage of endogenous plasma albumin crosses the intact blood–brain barrier (BBB), but plasma albumin can penetrate an open BBB in the case of brain injury.[19] Because albumin shows a high affinity for β-amyloid,[16] it could be one of the molecules related to the clearance of β-amyloid from the brain, and might be codeposited in senile plaques in brain injury and microhemorrhage.

After identifying the *APOE-ε4* as a risk for LOAD, it has been intriguing to consider the cause of AD: fatty acid transport or cholesterol metabolism? It has been shown that statins can substantially lower the risk of developing dementia including AD.[8] While statins are inhibitors of 3-hydroxy-3-methylglutaryl CoA (HMG-CoA) reductase, polyunsaturated fatty acids also inhibit HMG-CoA reductase activity.[20] This notion is also supported by evidence that animals with essential fatty acid deficiency show an increase in HMG-CoA reductase activity, which reverted to normalcy following the topical application of linolenic acid.[21] Fatty acid oxidation can facilitate the polymerization of tau,[22] and the antioxidant activity of β-amyloid could act in preventing polyunsaturated free fatty acids from oxidation.[23] Considering the notion that *in vitro* polyunsaturated free fatty acids stimulate the assembly of β-amyloid and tau filaments,[24] fatty acid environment could modify the development of AD pathology.

While it was noted that β-amyloid alters cellular cholesterol homeostasis,[25] it is likely that β-amyloid also participates in cellular fatty acid homeostasis, which could be an effective target in the prevention and therapy of LOAD, supported by evidence that docosahexaenoic acid provides protection from the impairment of learning ability in AD model rats.[26]

In conclusion, we found that the $(CA)_{11}$ allele of the intron 4 microsatellite was protective for LOAD. Furthermore, we showed a trend that the $(CA)_{11}$ allele is frequently found in non-demented subjects over 90 years. Since it was suggested that plasma albumin decreases with age,[27] the *ALB* gene could harbor genetic alterations targeted by aging factors.

ACKNOWLEDGMENTS

We thank Dr Yoshiaki Ikemura, Dr Yoshiaki Moto, Dr Yutaka Sawa, Dr Osamu Fujimoto, Dr Takeshi Matsubayashi, Dr Yoshiya Kato, Dr Ken Taniguchi and Dr Jyun-Ichiro Okuda for patient evaluations. This study was supported by a grant from the Research for the Future Program, Japan Society for the Promotion of Science (JSPS).

REFERENCES

1. Farrer LA, Cupples LA, Haines JL *et al.* Effects of age, sex, and ethnicity on the association between apolipoprotein E genotype and Alzheimer disease. A meta-analysis. APOE and Alzheimer Disease Meta Analysis Consortium. *JAMA* 1997; **278**: 1349–1356.
2. Strittmatter WJ, Saunders AM, Schmechel D *et al.* Apolipoprotein E: high-avidity binding to beta-amyloid and increased frequency of type 4 allele in late-onset familial Alzheimer disease. *Proc. Natl Acad. Sci. USA* 1993; **90**: 1977–1981.
3. Strittmatter WJ, Saunders AM, Goedert M *et al.* Isoform-specific interactions of apolipoprotein E with microtubule-associated protein tau: implications for Alzheimer disease. *Proc. Natl Acad. Sci. USA* 1994; **91**: 11183–11186.
4. Beffert U, Arguin C, Poirier J. The polymorphism in exon 3 of the low density lipoprotein receptor-related protein gene is weakly associated with Alzheimer's disease. *Neurosci. Lett.* 1999; **259**: 29–32.
5. Kang DE, Saitoh T, Chen X *et al.* Genetic association of the low-density lipoprotein receptor-related protein gene (LRP), an apolipoprotein E receptor, with late-onset Alzheimer's disease. *Neurology* 1997; **49**: 56–61.
6. Glaser C, Schulz S, Handschug K, Huse K, Birkenmeier G. Genetic and functional characteristics of the human in vivo LRP1/A2MR receptor suggested as a risk marker for Alzheimer's disease and other complex (degenerative) diseases. *Neurosci. Res.* 2004; **50**: 85–101.
7. Kang DE, Pietrzik CU, Baum L *et al.* Modulation of amyloid β-protein clearance and Alzheimer's disease susceptibility by the LDL receptor-related protein pathway. *J. Clin. Invest.* 2000; **106**: 1159–1166.
8. Jick H, Zornberg GL, Jick SS, Seshadri S, Drachman DA. Statins and the risk of dementia. *Lancet* 2000; **356**: 1627–1631.
9. Hoshino T, Kamino K, Matsumoto M. Dose of Apolipoprotein E-ε4 allele inversely correlates to plasma high-density lipoprotein cholesterol level in patients with Alzheimer's disease. *Neurobiol. Aging* 2002; **23**: 41–45.
10. Dietschy JM, Turley SD. Cholesterol metabolism in the brain. *Curr. Opin. Lipidol.* 2001; **12**: 105–112.
11. Björkhem I, Lütjohann D, Breuer O, Sakinis A, Wennmalm Å. Importance of a novel oxidative mechanism for elimination of brain cholesterol. Turnover of cholesterol and 24(S)-hydroxycholesterol in rat brain as measured with $^{18}O_2$ techniques in vivo and in vitro. *J. Biol. Chem.* 1997; **272**: 30 178–30 184.
12. Kölsch H, Lütjohann D, Ludwig M *et al.* Polymorphism in the cholesterol 24S-hydroxylase gene is associated with Alzheimer's disease. *Mol. Psychiatry* 2002; **7**: 899–902.
13. Papassotiropoulos A, Streffer JR, Tsolaki M *et al.* Increased brain β-amyloid load, phosphorylated tau, and risk of Alzheimer disease associated with an intronic CYP46 polymorphism. *Arch. Neurol.* 2003; **60**: 29–35.
14. Edmond J. Essential polyunsaturated fatty acids and the barrier to the brain: the components of a model for transport. *J. Mol. Neurosci.* 2001; **16**: 181–193.
15. Spector AA. Fatty acid binding to plasma albumin. *J. Lipid Res.* 1975; **16**: 165–179.
16. Biere AL, Ostaszewski B, Stimson ER, Hyman BT, Maggio JE, Selkoe DJ. Amyloid β-peptide is transported on lipoproteins and albumin in human plasma. *J. Biol. Chem.* 1996; **271**: 32 916–32 922.
17. McKhann G, Drachman D, Folstein M, Katzman R, Price D, Stadlan EM. Clinical diagnosis of Alzheimer's disease. Report of the NINCDS-ADRDA Work Group under the auspices of Department of Health and Human Services Task Force on Alzheimer's disease. *Neurology* 1984; **34**: 939–944.
18. Peters T Jr. Serum albumin: recent progress in the understanding of its structure and biosynthesis. *Clin. Chem.* 1977; **23**: 5–12.
19. Vorbrodt AW, Dobrogowska DH, Ueno M, Tarnawski M. A quantitative immunocytochemical study of blood–brain barrier to endogenous albumin in cerebral cortex and hippocampus of senescence-accelerated mice (SAM). *Folia Histochem. Cytobiol.* 1995; **33**: 229–237.
20. Field FJ, Albright EJ, Mathur SN. Effect of dietary n-3 fatty acids on HMG-CoA reductase and ACAT activities in liver and intestine of the rabbit. *J. Lipid Res.* 1987; **28**: 50–58.
21. Proksch E, Feingold KR, Elias PM. Epidermal HMG CoA reductase activity in essential fatty acid deficiency: barrier requirements rather than eicosanoid generation regulate cholesterol synthesis. *J. Invest. Dermatol.* 1992; **99**: 216–220.

22. Gamblin TC, King ME, Kuret J, Berry RW, Binder LI. Oxidative regulation of fatty acid-induced tau polymerization. *Biochemistry* 2000; **39**: 14 203–14 210.
23. Kontush A, Berndt C, Weber W *et al.* Amyloid-β is an antioxidant for lipoproteins in cerebrospinal fluid and plasma. *Free Radic. Biol. Med.* 2001; **30**: 119–128.
24. Wilson DM, Binder LI. Free fatty acids stimulate the polymerization of tau and amyloid β peptides. In vitro evidence for a common effector of pathogenesis in Alzheimer's disease. *Am. J. Pathol.* 1997; **150**: 2181–2195.
25. Liu Y, Peterson AD, Schubert D. Amyloid β peptide alters intracelluar vesicle trafficking and cholesterol homeostasis. *Proc. Natl Acad. Sci. USA* 1998; **95**: 13 266–13 271.
26. Hashimoto M, Hossain S, Shimada T *et al.* Docosahexaenoic acid provides protection from impairment of learning ability in Alzheimer's disease model rats. *J. Neurochem.* 2002; **81**: 1084–1091.
27. Ishiyama R, Osono Y, Ebihara Y, Niikawa O, Tani M, Nakamura Y. The changes in physico-chemical parameters obtained from apparently healthy aged people followed over ten years. *Jpn J. Geriatr. (Nippon Ronen Igakkai Zasshi)* 1993; **30**: 698–704 (in Japanese).

Psychiatry and Clinical Neurosciences (2006), **60**, S27–S33

Regular Article

Toll-like receptor 3 mediated hyperphosphorylation of tau in human SH-SY5Y neuroblastoma cells

BEGUM NURUN NESSA, MD,[1] TOSHIHISA TANAKA, MD, PhD,[1] KOUZIN KAMINO, MD, PhD,[1] GOLAM SADIK, PhD,[1] MD. ASHIK BIN ANSAR,[1] RYO KIMURA, PhD,[1] HISASHI TANII, MD, PhD,[2] MASAYASU OKOCHI, MD, PhD,[1] TAKASHI MORIHARA, MD, PhD,[1] SHINJI TAGAMI, MD, PhD,[1] TAKASHI KUDO, MD, PhD[1] AND MASATOSHI TAKEDA, MD, PhD[1]

[1]*Course of Advanced Medicine, Department of Post Genomics and Disease, Division of Psychiatry and Behavioral proteomics, Osaka University Graduate school of Medicine, Osaka, Japan,* [2]*Department of Psychiatry, Mie University, Mie, Japan*

Abstract Neurofibrillary tangles of abnormally phosphorylated tau are one of the characteristic pathological hallmarks of Alzheimer's disease (AD). In addition, immunological and inflammatory changes including complements and activated microglia are also common phenomena in AD. However, these pathological changes are yet to be interlinked in a common explainable background. In this study, the relevant mechanism of phosphorylation of tau protein and an innate immune signal transduction system were investigated. Toll-like receptor 3 (TLR3) is a receptor working in the innate immune system and its expression in the brain has already been reported. Total RNA was isolated from SH-SY5Y cells and reverse transcriptase polymerase chain reaction was done to see endogenous expression of TLR3 in SH-SY5Y cells that was further confirmed at protein level by Western blot analysis. Cells were treated with 50 μg/mL of polyinosinic–polycytidylic acid (pIpC), a synthetic analog of dsRNA and the changes of phosphorylation of tau protein were investigated. Further the level of phosphorylation of tau protein was investigated after the cells had been previously treated with 10 ng/mL of lipopolysaccharide (LPS) for 6 h to induce over-expression of TLR3. Increased phosphorylation of tau protein at PHF-1 site (Ser396/404), activation of Jun N-terminal kinase and p38 MAPK were observed in cells treated with pIpC. These effects were enhanced when cells were pretreated with LPS, a known transducer of TLR3. These data suggest that toll-like receptor 3, an innate immune molecule, might be a potential link to mediate hyperphosphorylation of tau in neurodegenerative processes of AD.

Key words Alzheimer's, disease, hyperphosphorylation of tau and toll-like receptor 3, innate immunity.

INTRODUCTION

Neurofibrillary tangles (NFTs) are pathological hallmarks of Alzheimer's disease (AD) and abnormally hyperphosphorylated tau is the major protein component of NFTs.[1–4] In addition, activation of immune cells such as activated microglia and accumulation of inflammation-associated proteins, including various cytokines and complements, are also a common phenomena associated with AD.[5–7] The etiopathogenesis of hyperphosphorylation of tau has been studied for ages by number of investigators. Numerous protein kinases and protein phosphatases have been implicated in the pathogenesis of aberrant phosphorylation of tau protein in the AD brain.[8–12] A recent study has suggested hyperphosphorylation of tau in cortical neurons to be mediated by interleukin-1 of activated microglia through p38-MAPK pathway thus linking activation of innate immune cells of CNS and hyperphosphorylation of tau.[13]

The evolutionarily ancient innate immune system provides the first line of host defense against a large variety of pathogens, tissue insults and also controls many aspects of the adaptive immune response.[14] Cells

Correspondence address: Toshihisa Tanaka, MD, PhD, Course of Advanced Medicine, Department of Post Genomics and Disease, Division of Psychiatry and Behavioral proteomics, Osaka University Graduate school of Medicine, 2-2 Yamadaoka Suita, Osaka 565-0871, Japan. Email: tanaka@psy.med.osaka-u.ac.jp

of the innate immune system recognize invariant pathogens associated with molecular patterns through a series of genetically conserved and stable cell surface receptors related to the *Drosophila* gene toll that are therefore referred to as toll- like receptors (TLR).[15] Broad expression of various TLRs (10 in number) has already been reported in the human brain.[16] Moreover activation of innate immunity in CNS is found to trigger neurodegeneration through a toll-like receptor 4-dependant pathway.[17]

We focused on TLR3, which responds to its two known ligands: double stranded RNA (dsRNA, replication intermediary for many viruses)[18] and endogenous mRNA (released from or associated with necrotic cells).[19] Upon binding with its ligand, TLR3 activates a variety of signaling pathways including activation of p38 MAP kinase and Jun N-terminal kinase (JNK).[18–20] Moreover subsclerosing pan encephalitis (SSPE), one of the known taupathies caused by the measles virus (RNA virus) has shown the evidence of neuronal loss and infiltration of inflammatory cells along with formation of NFTs.[21] Taken together, we hypothesized whether the ligand-mediated activation of TLR3 can induce hyperphosphorylation of tau through the activation of MAP kinases or not.

In the present study we evaluated the expression level of TLR3 in human SH-SY5Y neuroblastoma cell line and determined ligand-induced activation of TLR3 to mediate hyperphosphorylation of tau.

MATERIALS AND METHOD

Reagents

Polyinosinic–polycytidylic acid (pIpC) and lipopolysaccharide (LPS) from *Escherichia coli* 055:B5 were purchased from Sigma-Aldrich, Tokyo, Japan. PHF-1 antibody that can detect phosphorylated tau at Ser396/404 was a gift from Dr P. Davies (Albert Einstein University, New York, NY, USA). Anti-JNK/SAPK, anti phospho JNK/SAPK (Thr183/Tyr185), antip38/MAPK and antiphospho p38/MAPK (Thr180/Tyr182) were purchased from Cell Signaling Technology (MA, USA). Anti-TLR3 (rabbit polyclonal igG), Anti-TLR3 (mouse monoclonal igG), were purchased from Santa Cruz Biotechnology, Santa Cruz, CA, USA and CALBIOCHEM, San Diego, CA, USA, respectively. Antibodies against C-terminal and N-terminal of human TLR3 were purchased from ABGENT, San Diego, CA, USA.

Cell line and culture condition

SH-SY5Y human neuroblastoma cells were cultured in DMEM/F12 (Invitrogen, Carlsbad, CA, USA) supplemented with 5% fetal calf-serum (FCS) and were maintained at 37°C in a humid atmosphere containing 95% air/5% CO_2.

Cell treatment

Cells were treated with 50 μg/mL of pIpC for a different duration of time with or without the LPS (10 μg/mL) pretreatment for 6 h.

Rt-pcr

Total RNA was extracted from cultured cells using RNeasy® kit (Qiagen, Tokyo, Japan) according to the manufacturer's instruction. Total RNA (4 μg) was reversed transcribed using oligo (dT) primers with Thermo Script™ RT-PCR system (Invitrogen). To compare the mRNA levels among different RNA samples, RT was performed simultaneously using the reagents from a single master mix. Transcribed cDNA was used as a template for PCR amplification in a 50 μL reaction volume with Platinum® Taq DNA Polymerase (Invitrogen) for 35 cycles at 95°C for 45 s, 62°C for 40 s and 72°C for 1 min followed by a final extension for 10 min at 72°C. GAPDH was used as an internal control. PCR products were visualized on a 2% agarose gel by ethidium bromide staining. The TLR3 and GAPDH cDNA were amplified with the following primers: 5-TCCGTTGAGAAGAAGGTTTTCGGG-3 and 5-ATATCCTCCAGCCCTCCAAGTGGA-3 for TLR3, 5-CACAGTCCATGCCATCACTG-3 and 5-TACTCCTTGGAGGCCATGTG-3 for GAPDH.

Western blot

Cells were lyzed in 100 mM PIPES pH 6.8, 2 mM $MgCl_2$, 0.1 mM EDTA, 1 mM PMSF, 5 μg/mL aprotinine, 5 μg/mL leupeptine, 25 mM NaF, 1 mM Na3 VO4, 0.1% Triton-X100 on ice, and centrifuged at 200 000 × g for 30 min.

Supernatants were employed for Western blot analysis. Aliquots (50 μg) of the supernatants were separated by SDS-PAGE and transferred to PVDF membrane. As secondary antibodies, peroxides labeled antirabbit IgG were used and the membranes were developed by ECL (Amersham Bioscience, Buckinghamshire, UK).

RESULTS

We observed endogenous expression of TLR3 mRNA in SH-SY5Y cells by means of RT-PCR (Fig. 1a). Furthermore, expression of TLR3 at the protein level was confirmed by Western blot analysis (Fig. 1b). Lipopolysaccharide (LPS), which is known to induce

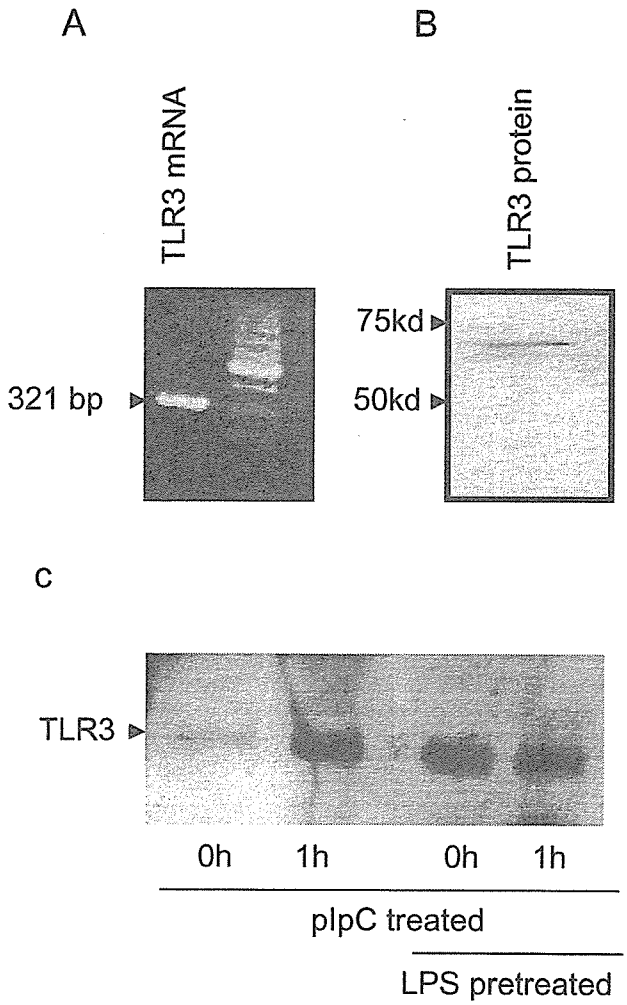

Figure 1. (A) Endogenous expression of TLR3 mRNA in SH-SY5Y cell line as evidenced by RT-PCR. Total RNA isolated from cultured SH-SY5Y cells were subjected to RT-PCR with specific primer for TLR3. (B) Endogenous expression of TLR3 protein in SH-SY5Y cell line as evidenced by Western blot analysis. (C) LPS induced over-expression of endogenous TLR3 in SH-SY5Y cells. Cells either pretreated with 10 ng/mL of LPS or without pretreatment (change of medium only) for 6 h, were treated with pIpC 50 μg/mL for the indicated number of hours. The level of expression of TLR3 protein was observed by Western blot using anti-TLR3 antibody. Data are representative of at least three separate experiments.

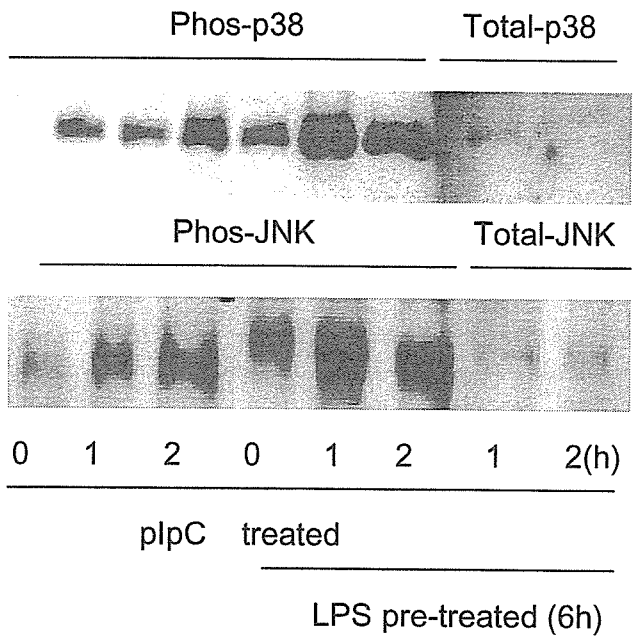

Figure 2. LPS-induced TLR3-mediated enhanced activation of p38-MAPK and JNK by pIpC. Cells either pretreated with 10 ng/mL of LPS or without pretreatment (change of medium only) for 6 h were treated with pIpC 50 μg/mL for the indicated number of hours. The level of phosphorylation of p38-MAPK was observed and compared with unphosphorylated total-p38 MAPK (upper panel) by Western blot analysis. Further level of phosphorylation of JNK was observed and compared with unphosphorylated total-JNK by Western blot analysis (lower panel). Data are representative of at least three separate experiments.

over-expression of TLR3 in many other tissues[18] was also found to upregulate TLR3 expression in SH-SY5Y cells (Fig. 1c). As is shown, LPS pretreatment for 6 h markedly increases the expression of TLR3 by pIpC at 0 h (Fig. 1c, lane 3) compared to pIpC treatment only (Fig. 1c, lane 1).

We then sought to elucidate whether LPS pretreated over-expressed TLR3 mediated enhanced activation of p38-MAPK and JNK by pIpC (Fig. 2). Only pIpC treatment increased activation of p38-MAPK (Fig. 2, upper panel lanes 1–3) and JNK (Fig. 2, lower panel, lanes 1–3) progressively at 1 h and 2 h. We used Phospho p38 and Phospho JNK antibody to detect activation of p38 MAPK and JNK, respectively. Moreover this activation was further enhanced when LPS pretreatment was done for 6 h followed by pIpC treatment (lanes 4–6). However, total p38-MAPK (Fig. 2, lanes 7, 8) and total JNK (Fig. 2, lanes 7, 8) did not show any difference even after LPS pretreatment.

Activation of p38 MAPK and JNK has been associated with stress response and more specifically with hyperphosphorylation of tau in AD. Since an elevation of phosphorylated p38 MAPK and phosphorylated JNK were observed in our experiment through pIpC-induced activation of TLR3 (Fig. 2), we tested whether activation of these kinases participate in the TLR3-mediated hyperphosphorylation of tau or not. Cells were either pretreated with LPS for 6 h to induce over-expression of TLR3 or with the change of medium fol-

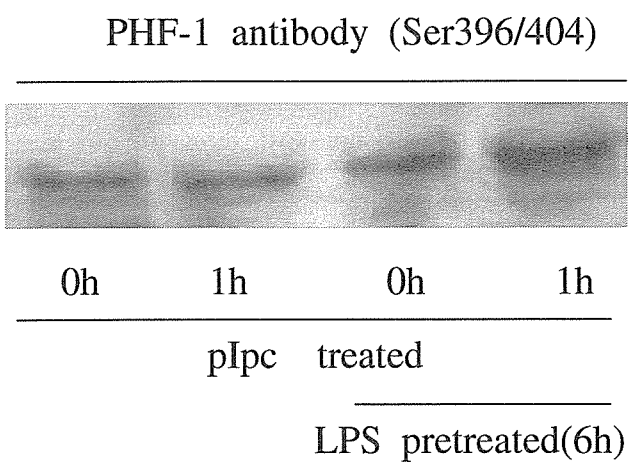

Figure 3. LPS-induced TLR3-mediated enhanced phosphorylation of tau by pIpC. Cells either pretreated with 10 ng/mL of LPS or without pretreatment (change of medium only) for 6 h, were treated with pIpC 50 μg/mL for the indicated number of hours. The level of phosphorylation of tau at ser396/404 was observed using PHF-1 antibody by Western blot analysis. Data are representative of at least three separate experiments.

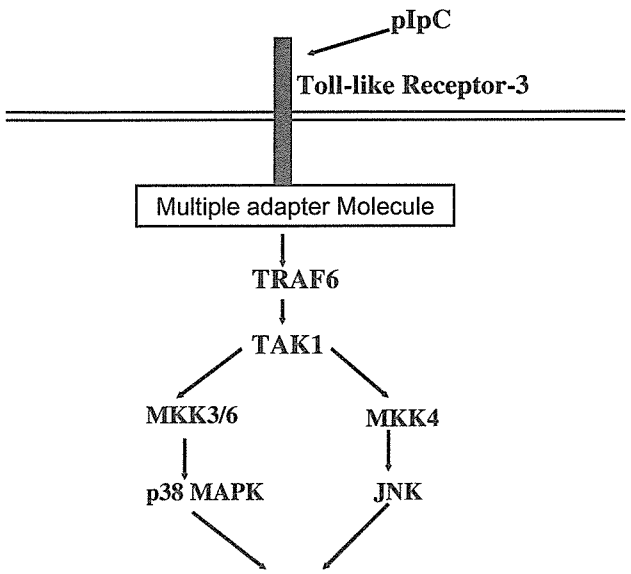

Figure 4. Schematic demonstration of intracellular signal transduction pathway of toll-like receptor-3 to mediated hyperphosphorylation of tau. Upon binding of dsRNA (ligand) to Trans membrane receptor, TLR3, multiple adaptor molecule are recruited to the receptor to form a complex to activate TRAF-6 (TNF receptor activated factor 6). Activated TRAF-6 transfers the signal to TAK-1 (TGF β activated kinase 1). Thus TAK-1 can activate MAPKKs (MAP kinase kinase), family of MKK3/6 and MKK4, which in turn activate the p38 and JNK pathway, respectively.

lowed by pIpC treatment. Hyperphosphorylation of tau was detected employing the PHF-1 antibody, which specifically detects ser396/404 phospho epitope of tau protein. We could see pIpC-induced TLR3-mediated hyperphosphorylation of tau (Fig. 3, lanes 1–2) which was further enhanced by LPS pretreatment (Fig. 3, lanes 3–4), indicating that ligand (pIpC)-mediated activation of TLR3 can mediate hyperphosphorylation of tau (Fig. 3).

The pIpC-induced TLR3-mediated signaling pathways was studied mainly in peripheral macrophages and had shown activation of TRAF-6 (TNF receptor-activated factor 6) through multiple adaptor molecules. When TRAF-6 is activated, it transfers the downstream signal to TAK-1 (TGF β activated kinase 1). Activated TAK-1 then leads to phosphorylation and activation of MAPKKs (MAP kinase kinases) family of MKK3/6 and MKK4, which in turn activate the p38 and JNK pathway, respectively. Thus, on the basis of the known signaling pathway of TLR3 in peripheral macrophages, we speculated the same loop of pathway to be working in human SH-SY5Y cell line to activate JNK and p38 MAPK to mediate hyperphosphorylation of tau (Fig. 4).

DISCUSSION

The current study reports that endogenous expression of TLR3 in SH-SY5Y cells and ligand-induced TLR3-mediated hyperphosphorylation of tau can be further enhanced by LPS pretreatment. To trace TLR3-induced signal transduction pathway mediating hyperphosphorylation of tau we evaluated two kinases: p38 MAPK and JNK. We observed that these two kinases are at least involved in ligand (pIpC)-induced TLR3-mediated hyperphosphorylation of tau.

Amyloid plaques and NTFs are two well-known pathological hallmarks of AD.[22,23] Moreover, a prominent innate immune response has been observed in association with pathological lesions of AD that includes activation of microglia, activation of complement, secretion of proinflammatory kinase such as interleukin (IL)-1β and tumor necrosis factor (TNF)-α; expression of the chemokines such as MIP-1α, MIP-1β and MCP-1 and the secretion of nitric oxide.[24,25] Recently, studies have shown that IL-1 released from activated microglia mediates hyperphosphorylation of tau in cortical neurons through the p38 MAPK pathway.[13,26] Moreover activated microglia has been correlated with neurofibrillary pathology,[27] including intracellular tau accumulation.[28,29] These investigations therefore indicate the involvement of innate immune activation in the pathway of aberrant phosphorylation

of tau. We focused on an innate immune receptor, TLR3, that is reported to be expressed in macrophage, astrocyte and oligodentrocyte in the human brain.[16] The current study reports the endogenous expression of TLR3 in SH-SY5Y cells. We also showed that ligand-induced TLR3 mediated hyperphosphorylation of tau in the SH-SY5Y cell line, which highlights the involvement of TLR3, an innate immune molecule in the pathogenesis of tau hyperphosphorylation. To date, two ligands have been reported to bind with TLR3. One is dsRNA[18] associated with viral infection and another is endogenous mRNA. Kariko *et al.* first reported that mRNA escaping from damaged tissue or contained within endocytosed cells is a potent host-derived ligand of TLR3.[19] Moreover RNA sequestration to NFTs and amyloid plaques in AD and other neurodegenerative diseases has been demonstrated by Ginsberg *et al.*[30–32] In addition, Marcinkiewicz *et al.*[33] had shown that immature plaques and dystrophic dendrites are capable of concentrating specific mRNA. Although the mechanism(s) by which RNA become sequestered to NFTs *in vivo* remains unknown, *in vitro* evidence suggests that RNA may act as a pathological chaperone to accelerate the aggregation of tau proteins into insoluble paired helical filaments.[34] However, the molecular mechanism of sequestration of this RNA and their role in the onset and progression of human neurodegenerative diseases are still not known. Given these precedents, it is reasonable to speculate that RNA released by necrotic cells or through phagocytes of necrotic cells in neurodegenerative and inflammatory process of AD could conceivably act as ligand to stimulate TLR3 signaling pathways, which may mediate hyperphosphorylation of tau and NFT formation. In our study, we used commercially available synthetic analog of dsRNA/pIpC as ligand of TLR3, considering the endogenous ligand (mRNA) would have mediated the same response. Moreover, one of the RNA groups of viruses (measles virus) causing SSPE characteristically had shown hyperphosphorylation of tau with NFT formation in association with neuronal loss, and infiltration of inflammatory cells.[35–37] Ultrastructurally, these NFTs are made of PHF identical to those seen in AD. However, the reason behind this association of virus infection with NFTs formation in SSPE still remains unclear. Taken together, it can be speculated that a common phenomena might be involved to mediate hyperphosphorylation of tau and NFT formation in these two diseases, with much clinical diversity but showing identical pathological features. Our *in vitro* study of ligand-induced TLR-3-mediated hyperphosphorylation of tau thus helps to shed some light on the role of an innate immune receptor, which might play a common role in the pathogenesis of NFT formation in various neurodegenerative taupathies such as AD and SSPE.

The pIpC-induced TLR3-mediated signal transduction pathway has been studied by various investigators however there remains more to investigate.[38,39] In brief, stimulation of TLR3 by a specific ligand induces nuclear transport of NF-kB and the activation of a set of Mitogen-activated protein kinases (MAPkinases) (extracellular signal regulated kinases (ERKs), JNK, and p38MAPK) through multiple signaling components or adaptor molecule. Since increased expression of active kinases, including JNK and p38 MAPK has been found in association with all the taupathies,[40] we sought whether these two kinases were also involved in the TLR3-mediated hyperphosphorylation of tau. In our study we observed pIpC induced activation of p38 MAPK and JNK. These activations were further enhanced when TLR3 were overexpressed by LPS pretreatment, thus indicating the activation of these two kinases in the pathway of TLR3-mediated hyperphosphorylation of tau by pIpC. However, we did not check other upstream signaling components such as TRAF/TAK/MKK, which would have shown more detail of the TLR3-mediated activation of JNK/p38MAPK to mediate hyperphosphorylation of tau in SH-SY5Y cells.

In conclusion, this study showed evidence that TLR3 might be a potential mechanistic link between innate immunity and hyperphosphorylation of tau. A better understanding of how innate immunity affects hyperphosphorylation of tau and neurodegeneration will help to develop a new diagnostic and therapeutic approach.

ACKNOWLEDGMENT

This work was supported by grant 16591136 from the Ministry of Education, Culture, Sports, Science and Technology, Japan.

REFERENCES

1. Grundke-Iqbal I, Iqbal K, Tung YC, Quinlan M, Wisniewski HM, Binder LI. Abnormal phosphorylation of microtubule associated protein tau (tau) in Alzheimers Cytoskeletal Pathology. *Proc. Natl Acad. Sci. USA* 1986; **83**: 4913–4917.
2. Iqbal K, Grundke-Iqbal I, Smith AJ, George L, Tung YC, Zaidi T. Identification and localization of tau peptide to paired helical filaments of Alzheimers disease. *Proc. Natl Acad. Sci. USA* 1989; **86**: 5646–5650.
3. Grundke-Iqbal I, Iqbal K, Quinlan M, Tung YC, Zaidi MS, Wisniewski HM. Microtubule associated protein tau A component of Alzheimers paired helical filaments. *J. Biol. Chem.* 1986; **261**: 6084–6089.

4. Iqbal K, Smith AJ, Zaidi T, Grundke-Iqbal I. Microtubule associated protein tau. Identification of a novel peptide from bovine brain. *FEBS Lett.* 1989; **248**: 87–91.
5. Griffin WS, Sheng JG, Roberts GW, Mrak RE. Interleukin-1 expression in different plaque types in Alzheimer's disease: significance in plaque evolution. *J. Neuropathol. Exp. Neurol.* 1995; **54**: 276–281.
6. Sheng JG, Mrak RE, Griffin WS. Microglial interleukin-1 alpha expression in brain regions in Alzheimer's disease: correlation with neuritic plaque distribution. *Neuropathol. Appl. Neurobiol.* 1995; **21**: 290–301.
7. Mrak RE, Griffin WS. Glia and their cytokines in progression of neurodegeneration. *Neurobiol. Aging* 2005; **26**: 349–354.
8. Gong CX, Grundke-Iqbal I, Iqbal I, Iqbal K. Dephosphorylation of Alzheimers disease abnormally phosphorylated tau by protein phosphatase-2A. *Neuroscience* 1994; **61**: 765–772.
9. Ishiguro K, Shiratsuchi A, Sato S. Glycogen synthase kinase 3 beta is identical to tau protein kinase 1 generating several epitopes of paired helical filaments. *FEBS Lett.* 1993; **325**: 167–172.
10. Tanaka T, Zhong J, Iqbal K, Trenkner E, Grundke Iqbal I. The regulation of phosphorylation of tau in SY5Y neuroblastoma cells. *FEBS Lett.* 1998; **426**: 248–254.
11. Roder HM, Eden PA, Ingram VM. Brain protein kinase PK40erk converts Tau into PHF like form as found in Alzheimers disease. *Biochem. Biophys. Res. Commun.* 1993; **193**: 639–664.
12. Ferrer I, Gomez-Isla T, Puig B *et al.* Current advances on different kinases involved in tau phosphorylation, and implication in alzheimers disease and tau pathies. *Curr. Alzheimer Res.* 2005; **1**: 3–18.
13. Li Y, Liu L, Barger SW, Griffin WST. Interleukin-1 mediates pathological effects of microglia on tau phosphorylation and on synaptophysin synthesis in cortical neurons through a p38-MAPK pathway. *J. Neurosci.* 2003; **23**: 1605–1611.
14. Medzhitov R, Janeway CA Jr. Innate immunity: impact on the adaptive immune response. *Curr. Opin. Immunol.* 1997; **9**: 4–9.
15. Medzhitov R, Janeway CA Jr. Innate immune recognition: mechanisms and pathways. *Immunol. Rev.* 2000; **173**: 89–97.
16. Bsibsi M, Ravid R, Gveric D, van Noort JM. Broad expression of Toll-like receptors in the human central nervous system. *J. Neuropathol. Exp. Neurol.* 2002; **61**: 1013–1021.
17. Lehnardt S, Massillon L, Follett P *et al.* Activation of innate immunity in the CNS triggers neurodegeneration through a Toll-like receptor 4-dependent pathway. *Proc. Natl Acad. Sci. USA* 2003; **100**: 8514–8519.
18. Alexopoulou L, Holt AC, Medzhitov R, Flavel RA. Recognition of double-stranded RNA and activation of NF-kappaB by Toll-like receptor 3. *Nature* 2001; **413**: 732–738.
19. Kariko K, Ni H, Capodici J, Lamphier M, Weissman D. mRNA is an endogenous ligand for Toll-like receptor 3. *J. Biol. Chem.* 2004; **279**: 12542–12550.
20. Chu WM, Ostertag D, Li ZW *et al.* JNK2 and IKKβ are required for activating the innate response to viral infection. *Immunity* 1999; **11**: 721–731.
21. McQuaid S, Allen IV, McMahon J, Kirk J. Association of measles virus with neurofibrillary tangles in subacute sclerosing panencephalitis: a combined in situ hybridization and immunocytochemical investigation. *Neuropathol. Appl. Neurobiol.* 1994; **20**: 103–110.
22. Selkoe DJ. Cell biology of amyloid beta protein precursor and the mechanism of Alzheimers disease. *Annu. Rev. Cell Biol.* 1994; **10**: 373–403.
23. Schmidt ML, DiDario AG, Otvos L *et al.* Plaque-associated neuronal proteins: a recurrent motif in neuritic amyloid deposits throughout diverse cortical areas of the Alzheimer's disease brain. *Exp. Neurol.* 1994; **130**: 311–322.
24. Monsonego A, Weiner HL. Immunotherapeutic approaches to Alzheimer's disease. *Science* 2003; **302**: 834–838.
25. Ringheim GE, Conant K. Neurodegenerative disease and the neuroimmune axis (Alzheimer's and Parkinson's disease, and viral infections). *J. Neuroimmunol.* 2004; **147**: 43–49.
26. Sheng JG, Jones RA, Zhou XQ *et al.* Interleukin-1 promotion of MAPK-p38 overexpression in experimental animals and in Alzheimer's disease: potential significance for tau protein phosphorylation. *Neurochem. Int.* 2001; **39**: 341–348.
27. DiPatre PL, Gelman BB. Microglial cell activation in aging and Alzheimer disease: partial linkage with neurofibrillary tangle burden in the hippocampus. *J. Neuropathol. Exp. Neurol.* 1997; **56**: 143–149.
28. Sheng JG, Mrak RE, Griffin WS. Glial–neuronal interactions in Alzheimer disease: progressive association of IL-1alpha+ microglia and S100beta+ astrocytes with neurofibrillary tangle stages. *Acta Neuropathol. (Berl)* 1997; **94**: 1–5.
29. Sheng JG, Mrak RE, Griffin WS. Neuritic plaque evolution in Alzheimer's disease is accompanied by transition of activated microglia from primed to enlarged to phagocytic forms. *J. Neuropathol. Exp. Neurol.* 1997; **56**: 285–290.
30. Ginsberg SD, Crino PB, Lee VM, Eberwine JH, Trojanowski JQ. Sequestration of RNA in Alzheimer's disease neurofibrillary tangles and senile plaques. *Ann. Neurol.* 1997; **41**: 200–209.
31. Ginsberg SD, Galvin JE, Chiu TS, Lee VM, Masliah E, Trojanowski JQ. RNA sequestration to pathological lesions of neurodegenerative diseases. *Acta Neuropathol. (Berl)* 1998; **96**: 487–494.
32. Ginsberg SD, Crino PB, Hemby SE *et al.* Predominance of neuronal mRNAs in individual Alzheimer's disease senile plaques. *Ann. Neurol.* 1999; **45**: 174–181.
33. Marcinkiewicz M. Beta APP and furin mRNA concentrates in immature senile plaques in the brain of Alzheimer patients. *J. Neuropathol. Exp. Neurol.* 2002; **61**: 815–829.
34. Kampers T, Friedhoff P, Biernat J, Mandelkow EM, Mandelkow E. RNA stimulates aggregation of microtu-

bule-associated protein tau into Alzheimer-like paired helical filaments. *FEBS Lett.* 1996; **399**: 344–349.
35. Mandybur TI, Nagpaul AS, Pappas Z, Niklowitz WJ. Alzheimer neurofibrillary change in subacute sclerosing panencephalitis. *Ann. Neurol.* 1977; **1**: 103–107.
36. McQuaid S, Allen IV, McMahon J, Kirk J. Association of measles virus with neurofibrillary tangles in subacute sclerosing panencephalitis: a combined in situ hybridization and immunocytochemical investigation. *Neuropathol. Appl. Neurobiol.* 1994; **20**: 103–110.
37. Mandybur TI. The distribution of Alzheimer's neurofibrillary tangles and gliosis in chronic subacute sclerosing panencephalitis. *Acta Neuropathol. (Berl)* 1990; **80**: 307–310.
38. Jiang Z, Zamanian-Daryoush M, Nie H, Silva AM, Williams BR, Li X. Poly (I-C)-induced Toll-like receptor 3 (TLR3)-mediated activation of NFkappa B and MAP kinase is through an interleukin-1 receptor-associated kinase (IRAK)-independent pathway employing the signaling components TLR3-TRAF6-TAK1-TAB2-PKR. *J. Biol. Chem.* 2003; **278**: 16 713–16 719.
39. Meylan E, Burns K, Hofmann K *et al.* RIP1 is an essential mediator of Toll-like receptor 3-induced NF-kappa B activation. *Nat. Immunol.* 2004; **5**: 503–507.
40. Ferrer I, Gomez-Isla T, Puig B *et al.* Current advances on different kinases involved in tau phosphorylation, and implications in Alzheimer's disease and tauopathies. *Curr. Alzheimer Res.* 2005; **2**: 3–18.

Presenilin-Dependent γ-Secretase on Plasma Membrane and Endosomes Is Functionally Distinct†

Akio Fukumori,‡,§ Masayasu Okochi,*,‡,§ Shinji Tagami,‡,§ Jingwei Jiang,§ Naohiro Itoh,§ Taisuke Nakayama,§ Kanta Yanagida,§ Yoshiko Ishizuka-Katsura,§ Takashi Morihara,§ Kojin Kamino,§ Toshihisa Tanaka,§ Takashi Kudo,§ Hisashi Tanii,§ Akiko Ikuta,§ Christian Haass,|| and Masatoshi Takeda§

Division of Psychiatry and Behavioral Proteomics, Department of Post-Genomics and Diseases, Osaka University Graduate School of Medicine, Osaka, Japan, and Adolf Butenandt Institute, Department of Biochemistry, Laboratory for Alzheimer's and Parkinson's Disease Research, Ludwig-Maximilians University, Munich, Germany

Received November 25, 2005; Revised Manuscript Received February 25, 2006

ABSTRACT: The presenilin (PS)/γ-secretase complex, which contains not only PS but also Aph-1, PEN-2, and nicastrin, mediates proteolysis of the transmembrane domain of β-amyloid protein precursor (βAPP). Intramembrane proteolysis occurs at the interface between the membrane and cytosol (ε-site) and near the middle of the transmembrane domain (γ-site), generating the βAPP intracellular domain (AICD) and Alzheimer disease-associated Aβ, respectively. Both cleavage sites exhibit some diversity. Changes in the precision of γ-cleavage, which potentially results in secretion of pathogenic Aβ42, have been intensively studied, while those of ε-cleavage have not. Although a number of PS-associated factors have been identified, it is unclear whether any of them physiologically regulate the precision of cleavage by PS/γ-secretase. Moreover, there is currently no clear evidence of whether PS/γ-secretase function differs according to the subcellular site. Here, we show that endocytosis affects the precision of PS-dependent ε-cleavage in cell culture. Relative production of longer AICDε49 increases on the plasma membrane, whereas that of shorter AICDε51 increases on endosomes; however, this occurs without a concomitant major change in the precision of cleavage at γ-sites. Moreover, very similar changes in the precision of ε-cleavage are induced by alteration of the pH. Our findings demonstrate that the precision of ε-cleavage by PS/γ-secretase changes depending upon the conditions and the subcellular location. These results suggest that the precision of cleavage by the PS/γ-secretase complex may be physiologically regulated by the subcellular location and conditions.

Intramembrane proteolysis by presenilin (PS)/γ-secretase plays a key role in both Alzheimer disease (AD)[1] and regulated intramembrane proteolysis (RIP) signaling (*1*). At least two PS-dependent cleavages occur in the transmembrane domains of substrates such as β-amyloid protein precursor (βAPP), Notch, and CD44 ("dual cleavage"): one near the middle of the transmembrane domain (TM-N) (*2*−*5*) and the other on the border between the transmembrane domain and cytosol (TM-C) (*6*−*10*). The cleavage at the TM-N site of βAPP (γ-cleavage) is essential for Aβ generation and is closely related to AD (*2*, *11*). On the other hand, the cleavage at the TM-C site, including that in Notch-1 (S3-cleavage), generates ICDs (*i*ntracellular *c*ytoplasmic *d*omains) and is involved in RIP signaling (*1*).

In PS-dependent proteolysis, there is some diversity in the specific sites of cleavage (*3*, *5*, *7*−*9*, *11*). A change in cleavage precision can have an important effect on the pathogenesis of AD because Aβ42, a causative factor in AD, is generated by one of the types of γ-cleavage (*2*, *11*). Much time and effort have therefore been dedicated to understanding how the precise site of cleavage is determined. Most familial AD-associated PS and βAPP mutants affect the precision of γ-cleavage (*11*). Because such changes in the precision of γ-cleavage have not been observed in other conditions, it had been generally believed that the precision of this cleavage is not easily changed (*11*). Recent studies, however, have revealed that some chemicals including NSAIDs (*n*onsteroidal *a*nti*i*nflammatory *d*rug*s*) (*12*, *13*) up- or downregulate pathological Aβ42, indicating that the precision of this cleavage by PS/γ-secretase may change under certain circumstances (*14*). Notably, however, corresponding changes in the precision of ε-cleavage have not been examined.

ICDs including that of βAPP (AICD) and Notch (NICD) are generated by ε- and S3-cleavage at TM-C, respectively (*1*). ICDs are generally involved in translocation of signaling

† This work was supported by the Program for the Promotion of Fundamental Studies in Health Sciences of the National Institute of Biomedical Innovation (05-26), by Grants-in-Aid for Scientific Research on Priority Areas−Advanced Brain Science Project and for KAKENHI from the Ministry of Education, Culture, Sports, Science, and Technology of Japan, and by Grants-in-Aid from the Ministry of Health, Labor, and Welfare of Japan.

* To whom correspondence should be addressed. Tel: 81-6-6879-3053. Fax: 81-6-6879-3059. E-mail: mokochi@psy.med.osaka-u.ac.jp.

‡ Equal contributions.

§ Osaka University Graduate School of Medicine.

|| Ludwig-Maximilians University.

[1] Abbreviations: Aβ, amyloid-β peptide; AD, Alzheimer disease; AICD, βAPP intracellular cytoplasmic domain; βAPP, β-amyloid protein precursor; CMF, crude membrane fraction; CTF, carboxyl-terminal fragment; Dyn-1, dynamin-1; IP-MS, immunoprecipitation−mass spectroscopy; K293, human embryonic kidney 293; PM, plasma membrane; PS, presenilin; sw, Swedish mutant; TM-C, the border between the transmembrane domain and cytosol.

10.1021/bi052412w CCC: $33.50
Published on Web 03/28/2006

molecules to the nucleus to activate target genes in RIP signaling (*1*). Although, like γ-cleavage, ε-cleavage also exhibits diversity (*7*−*9*), the details of this diversity and the characteristics of the cleavage remain to be clarified. Both ε- and γ-cleavages are mediated by PS/γ-secretase (*2*), but whether the processes that determine the variety and the precision of these cleavages are common remains controversial. For example, it has been shown that ε-cleavage sites are associated with γ-cleavage sites (*7*, *15*, *16*); however, mutagenesis studies show that ε- and γ-cleavages are mediated by a distinct process (*17*).

PS is the proteolytic active center in the PS/γ-secretase protein complex (*2*, *18*). To exert its proteolytic function, PS must form a complex with at least nicastrin (*19*), PEN-2 (*20*), and APH-1 (*2*, *20*). Other factors that physiologically affect proteolysis, including the precision of cleavage, have not yet been identified. In contrast to other subcellular locations, AD-associated Aβ42 is produced in the ER without concomitant production of Aβ40. However, since this is not mediated by PS (*21*, *22*), whether the precision of PS-dependent proteolysis changes within cells depending on location or conditions remains unresolved.

In this study, using a cell-free γ-secretase assay, we examined whether the precision of cleavage by PS/γ-secretase is affected by its subcellular location. We demonstrate that, unlike γ-cleavage, ε-cleavage precision can drastically change depending on subcellular location and the pH. Relative cleavage at the ε51 site is more prone to occur on endosomes than on plasma membrane (PM) and at lower pH. In contrast, relative cleavage at the ε49 site is more likely to occur on PM than on endosomes and at higher pH. These results suggest that PS-dependent γ-secretase on plasma membrane and endosomes is functionally distinct.

MATERIALS AND METHODS

Antibodies. Rabbit antiserum 6618 was raised against a synthetic peptide KMQQNGYENPTYKFFEQMQN, which corresponds to the C-terminus of βAPP according to the methods described (*23*). The following antibodies were purchased from commercial sources: anti-Aβ antibody 4G8 (Senetec PLC), anti-Na−K ATPase (Upstate Biotechnology), anti-early endosome antigen 1 (BD Transduction Laboratories), anti-nicastrin (Sigma-Aldrich), anti-GM130 (BD Transduction Laboratories), and anti-tubulin (Santa Cruz Biotechnology). Also, antibody 12CA5 (Roche Diagnostics Inc.) was used to detect the N-terminal hemagglutinin-tagged dynamin-1 (Dyn-1) K44A mutant.

Cell Culture and cDNA Construct. Human embryonic kidney 293 (K293) cells stably expressing wild-type βAPP, wild-type PS1/βAPP Swedish (sw) mutant (*24*), or PS1 D385N/βAPP sw (*25*) were described previously. HeLa cells expressing Dyn-1 K44A under control of a tetracycline transactivator were kindly provided by Dr. Sandra L. Schmid (Scripps Institute, La Jolla, CA) (*26*). HeLa cells stably expressing βAPP sw were cultured without tetracycline (Sigma-Aldrich) for 48 h to induce expression of Dyn-1 K44A.

Membrane Fractionation and Cell-Free γ-Secretase Assay. The collected cells were homogenized with a Teflon homogenizer (20 strokes) in homogenization buffer (0.25 M sucrose and 10 mM HEPES, pH 7.4) containing a protease inhibitor cocktail (Roche) (*27*). The homogenate was centrifuged at 1000*g* for 5 min to remove nuclei and cell debris, followed by further centrifugation of the supernatant fraction at 100000*g* for 1 h. Following a single wash with homogenization buffer, the resulting precipitate was collected as the CMF and frozen in liquid nitrogen. Upon use, the frozen CMF samples were resuspended and immediately incubated in the reaction buffer [150 mM sodium citrate buffer (pH 5.0−7.4) containing 5 mM 1,10-phenanthroline (Sigma-Aldrich) and a 4× concentration of protease inhibitor cocktail (Roche)] for 20 min at 37 °C (cell-free incubation) (*28*, *29*). The reaction was terminated by placing the samples on ice.

Subcellular Fractionation. Linear gradients of 2.5−25% iodixanol (Optiprep; AXIS-SHIELD) were prepared. Postnuclear supernatant fractions from 24 dishes (ϕ = 14 cm) were loaded on the top of the gradient, followed by centrifugation for 3 h at 130000*g*. Each fraction was diluted with three volumes of homogenization buffer and centrifuged for 1 h at 100000*g* to precipitate the membranes. The precipitated membrane was used in cell-free γ-secretase assays or in immunoblots for marker proteins.

Metabolic Labeling. Following methionine starvation for 40 min, cells were metabolically labeled with 400 μCi of [^{35}S]methionine (Redivue Promix; Amersham Pharmacia Biotech) in methionine-free MEM for 20 min and chased for 30 min in DMEM containing 10% FBS and excess unlabeled methionine.

Immunoprecipitation/Autoradiography Analysis. Metabolically labeled CMF was lysed in RIPA buffer (1% Triton X-100, 0.5% sodium deoxycholate, and 0.1% SDS) containing a protease inhibitor mix (Sigma-Aldrich). The cell lysates were centrifuged at 10000*g* for 15 min, and the supernatant fractions were immunoprecipitated with 6618 antiserum for the detection of the C-terminal stub and de novo AICD. Following 10−20% Tris−tricine SDS−PAGE (Invitrogen), the gels were dried and analyzed by autoradiography (*3*).

Immunoprecipitation/Mass Spectroscopy (IP-MS) Analysis. IP-MS analysis was carried out as described previously (*3*). Following cell-free incubation, the CMF was sonicated four times for 10 s and then centrifuged at 100000*g* for 1 h. The supernatant were immunoprecipitated for 4 h at 4 °C in IP-MS buffer [140 mM NaCl, 0.1% *n*-octyl glucoside, 10 mM Tris-HCl (pH 8.0), 5 mM EDTA, and a protease inhibitor mix (Sigma-Aldrich)]. The heights of the MS peaks and molecular weights were calibrated using ubiquitin and/or bovine insulin β-chain as standards (Sigma-Aldrich). The relative peak heights were semiquantitatively analyzed (see Figure 3 in Supporting Information).

Immunoprecipitation/Immunoblot Analysis. Following cell-free incubation, the fractions were immunoprecipitated for 10 h at 4 °C in IP-MS buffer. After SDS−PAGE, the separated proteins were transferred to a PVDF or nitrocellulose (for detection of Aβ) membrane and probed with the indicated antibodies (*30*). The nitrocellulose membrane was heated for 10 min in boiling PBS before blocking. AICD and Aβ levels were semiquantified by chemiluminescence using an LAS3000 scanner and Multi Gauge Ver3.0 software (Fujifilm).

Transferrin Uptake Assay. To determine the level of internalized transferrin, the treated cells were washed three times in Hank's balanced salt solution (Sigma-Aldrich), pH 7.4, and then treated for 7 min at 37 °C with 8 μg/mL biotin−

transferrin (Sigma-Aldrich) in conditioned medium. To remove remaining surface-bound biotin−transferrin, cells were washed three times with Hank's balanced salt solution, pH 4.0. To determine the level of surface-bound transferrin, the treated cells were incubated for 30 min with biotin−transferrin at 4 °C and washed three times with Hank's balanced salt solution, pH 7.4 (*26*). The resulting cell lysates were separated by SDS−PAGE and transferred to the PVDF membrane. Biotin−transferrin was detected by neutravidin−horseradish peroxidase (Pierce). The level of endocytosis in each condition was expressed as of the ratio of internalized vs surface-bound transferrin (*31*).

RESULTS

The Cell-Free Assay Constitutes Bona Fide ϵ- and γ-Cleavages by PS/γ-Secretase. βAPP, a type 1 transmembrane protein, undergoes PS-dependent proteolysis in its transmembrane domain, following "shedding" of the extracellular domain at β- or α-sites (*11*). The intramembrane proteolysis is composed of at least two distinct proteolytic cleavages (dual cleavage), namely, at the ϵ- and γ-sites (Figure 1A) (*2*).

To determine whether the precision of cleavage in intramembrane proteolysis by each PS/γ-secretase is homogeneous in cells, we established a cell-free γ-secretase assay using a detergent-free membrane fraction (Figure 1) (*28*). First, de novo AICD generation from carboxyl-terminal fragment (CTF) stubs of βAPP was analyzed (Figure 1B,C). Following a 20 min metabolic labeling of K293 cells stably expressing βAPP sw and a 30 min chase, we extracted CMFs from the cells and incubated them under various conditions (cell-free incubation). To detect the C-terminus of βAPP, cell lysates were immunoprecipitated with rabbit antiserum 6618, separated by SDS−PAGE, and analyzed by autoradiography. As shown in Figure 1B, during cell-free incubation of the purified CMF, radiolabeled CTF stubs of βAPP rapidly underwent endoproteolysis and concomitantly generated labeled AICD. Termination of the PS function by either exogenous expression of the PS1 dominant negative mutant (D385N) (*32*) or by addition of a specific γ-secretase inhibitor to CMF (Figure 1C) inhibited generation of AICD.

We next examined the precision of both ϵ- and γ-cleavages in the cell-free assay using IP-MS analysis (Figure 1D). We first examined the molecular species of AICD generated during cell-free incubation. The IP-MS analysis showed that the MS profile of AICD was consistent with that previously reported (Figure 1D, left panel) (*7*−*9*). In addition, the MS spectrum of Aβ generated during cell-free incubation (Figure 1D, right panel) was almost identical to that of Aβ present in the conditioned medium just before extraction of the CMF (data not shown). We therefore conclude that the cleavages in the cell-free assay constitute bona fide PS-dependent ϵ- and γ-cleavages (Figure 1E).

The Precision of ϵ-Cleavage Drastically Changes upon Inhibition of Endocytosis. Proteolysis by PS/γ-secretase occurs on cell organelles including the PM and endosomes before and after endocytosis (*33*). Here, we focused on whether the precision of ϵ- and γ-cleavage changes upon inhibition of endocytosis. To inhibit endocytosis, we used the "tet-off system" (Clontech) in which the expression of the dynamin-1 (Dyn-1) dominant negative mutant K44A is

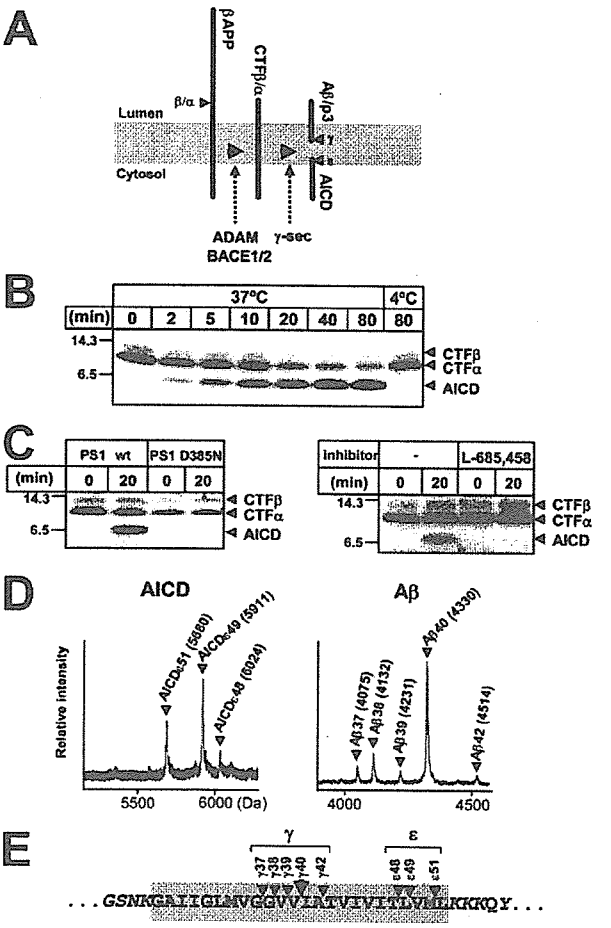

FIGURE 1: Generation of de novo AICD and Aβ in the cell-free γ-secretase assay. (A) Schematic representation of dual cleavage of the βAPP transmembrane domain. See Results for details. (B) Analysis of cell-free γ-secretase assay products by immunoprecipitation/autoradiography using CMF from cells stably expressing βAPP sw. Note that the ~7 kDa product (AICD) was generated over time along with a concurrent reduction in the level of substrates (CTF stubs of βAPP). (C) Analysis of cell-free γ-secretase assay products by immunoprecipitation/autoradiography using CMFs from (i) cells expressing a dominant negative PS1 mutant (PS1 D385N) or (ii) cells treated with or without 10 μM L685,458. (D) Molecular species of de novo AICD and Aβ generated in the cell-free assay. Molecular weights of de novo AICD (left panel) and Aβ (right panel) are shown. Following a 20 min cell-free incubation, the soluble fraction of CMF was immunoprecipitated with antibody 6618 (left panel) or 4G8 (right panel). Panels B−D show representative data from more than three independent experiments. (E) Schematic representation of the ϵ- and γ-cleavages of βAPP. Arrowheads indicate the cleavage sites found in the assay.

induced by tetracycline withdrawal (tet (−) treatment) in HeLa cells (Figure 2A) (*26*). We first examined the extent to which this mutant suppresses endocytosis of the transferrin receptor. We found that expression of Dyn-1 K44A inhibited the intracellular uptake of biotinylated transferrin (Figure 1 in Supporting Information) by approximately 87 ± 2% (Figure 2B).

Next, we analyzed the ϵ-cleavage in the cell-free γ-secretase assay using CMF from cells cultured with or without tetracycline (Figure 2C,D). Unlike the analysis of K293 cells, the mass spectral analysis showed that AICDϵ51 was a major species formed by CMF from HeLa cells stably expressing

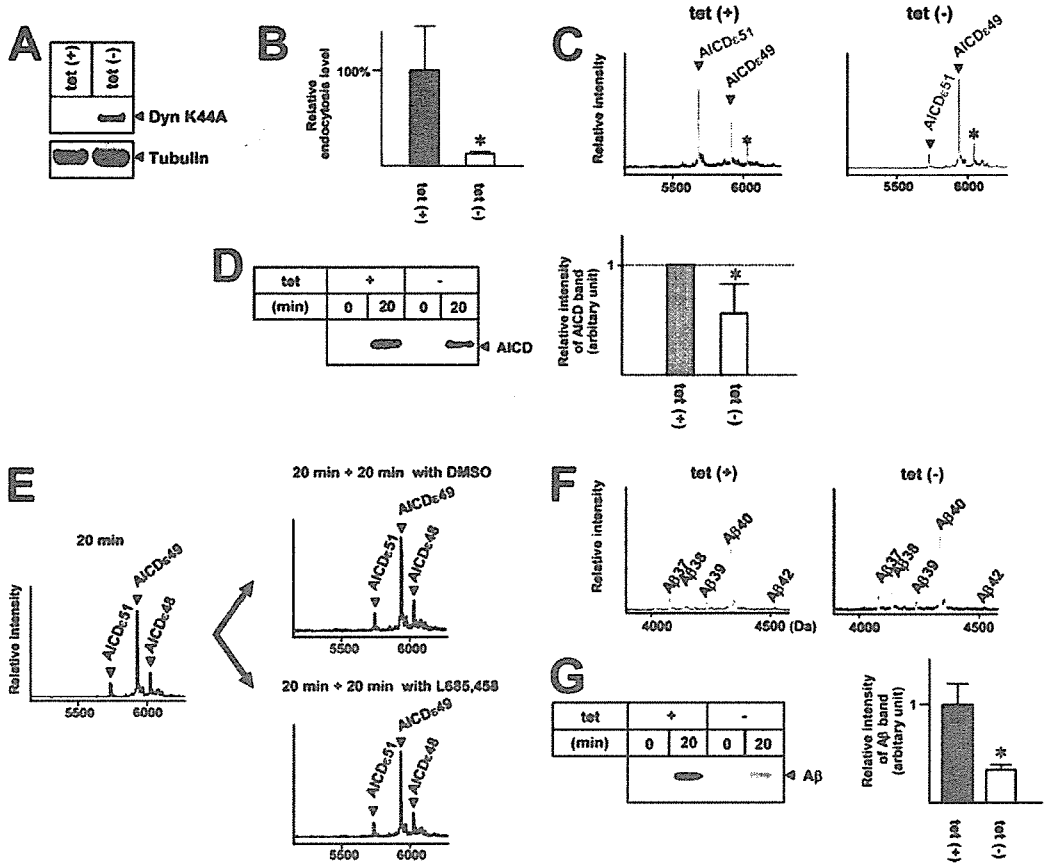

FIGURE 2: Effects of Dyn-1 K44A expression in HeLa cells on the cell-free γ-secretase assay. (A) Induction of Dyn-1 K44A expression. Cells were treated without (−) or with (+) tetracycline, and cell lysates were immunoblotted with 12CA5 (upper panel) or anti-tubulin (lower panel). The results show that Dyn-1 K44A is induced by removal of tetracycline. (B) Inhibition of endocytosis by Dyn-1 K44A expression. The ratio of internalized transferrin at 37 °C to cell surface bound transferrin at 4 °C in cells not expressing Dyn-1 K44A (tet(+)) was defined as 100%. The ratio of endocytosis decreased to 13 ± 2% when the expression of the mutant was induced (tet(−)). The asterisk indicates statistical significance ($P < 0.05$ by Student's *t*-test). (C) Mass spectra of cell-free generated AICD species. The CMFs from HeLa cells expressing βAPP sw cultured with or without tetracycline were incubated in the cell-free assay. Asterisks indicate the AICDε48 species. (D) The level of AICDs generated in the cell-free assay. The AICDs generated in cell-free assays were immunoprecipitated and immunoblotted with the 6618 antiserum (left panel). The intensity of each AICD band was measured by chemiluminescence (right panel). Generation of de novo AICDs was defined as the difference of the AICD band intensities with or without a 20 min cell-free incubation. The asterisk indicates statistical significance ($P < 0.01$ by Student's *t*-test). (E) Molecular species of AICD observed after a first (left panel) and a second 20 min incubation with L685,458 (lower right panel) or vehicle control DMSO (upper right panel) using CMF from HeLa cells expressing βAPP sw cultured without tetracycline. (F) Mass spectra of the Aβ species generated in the cell-free reaction. The samples were the same as those analyzed in panel C. (G) The level of Aβ produced in the cell-free assay. The Aβ generated in the cell-free assay was analyzed by immunoprecipitation, followed by immunoblotting with the 4G8 antibody (left panel). The intensity of each Aβ band was measured by chemiluminescence (right panel). The asterisk indicates statistical significance ($P < 0.01$ by Student's *t*-test). In (A), (C), (E), and (F) and in the left panels of (D) and (G), the results are representative data of more than three independent experiments. The results in (B) and the right panels of (D) and (G) indicate the means ± standard deviations of at least triplicate determinations. tet = tetracycline.

βAPP sw in our cell-free assay (Figure 2C, left panel, and Figure 3A, right panel). Surprisingly, expression of Dyn-1 K44A greatly increased the peak height of AICDε49 relative to that of AICDε51, indicating a change in the precision of ε-cleavage upon inhibition of endocytosis (Figure 2C; see also Table 1). A very similar large relative increase of the peak height of AICDε49 compared to that of AICDε51 was also observed upon addition of 100 nM bafilomycin A1 (Figure 2B in Supporting Information), which inhibited endocytosis by approximately 69 ± 5% (Figures 1 and 2A in Supporting Information) (*34*). Moreover, we found that the relative ratio of the AICDε49 peak height to that of AICDε51 semiquantitatively correlated with the relative amount of each AICDε49 species, indicating that AICDε49 and AICDε51 have similar ionization efficiencies in the matrix-associated laser desorption ionization/time-of-flight mass spectrometry (see Figure 3 in Supporting Information). We also examined whether the level of ε-cleavage changes upon inhibition of endocytosis by immunoblotting (Figure 2D). We detected a significant decrease in intensity of the AICD band upon Dyn-1 K44A expression, indicating that the level of ε-cleavage decreases upon inhibition of endocytosis. These findings suggest that inhibition of endocytosis causes a drastic change in the precision of ε-cleavage.

We further investigated whether both AICDε51 and AICDε49 are, indeed, direct products of PS/γ-secretase. We first generated de novo AICD by a 20 min cell-free incubation (Figure 2E, left panel). The solution was further incubated for 20 min with (Figure 2E, lower right panel) or without (Figure 2E, upper right panel) the γ-secretase

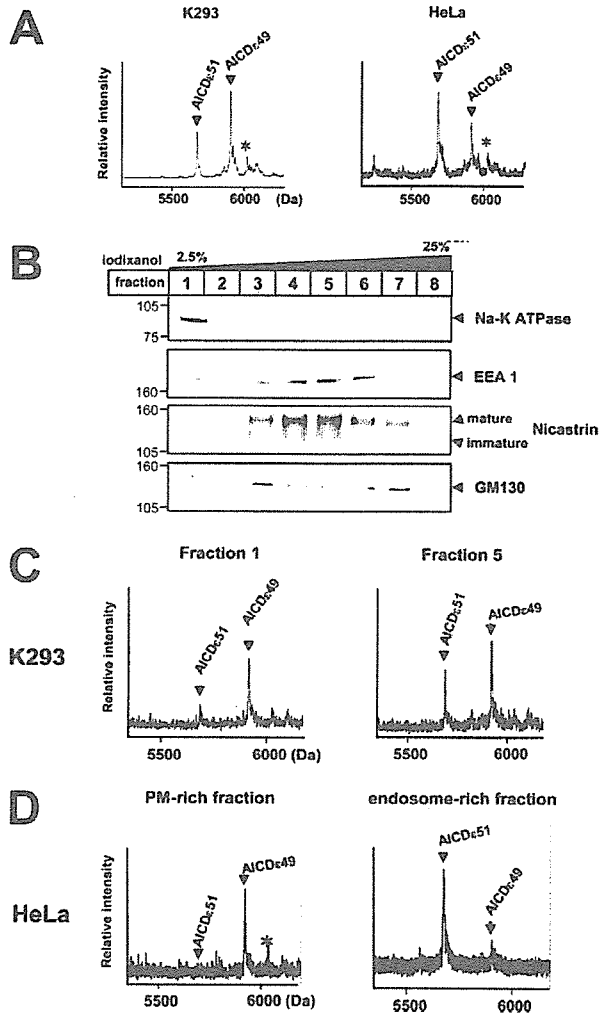

FIGURE 3: Cell-free γ-secretase assay using PM- and endosome-rich fractions. (A) Mass spectra of de novo AICD generated in the cell-free assay using whole CMFs from K293 (left panel) and HeLa (right panel) cells. Asterisks indicate AICDϵ48 species. (B) Postnuclear supernatant fractions of βAPP sw-expressing K293 cells were separated by iodixanol gradient centrifugation and analyzed by immunoblotting using antibodies to organelle marker proteins. (C) Mass spectra of de novo AICD generated by fractions 1 and 5 from K293 cells. (D) Mass spectra of de novo AICD generated by PM- or endosome-rich fractions from HeLa cells expressing βAPP sw. Results in (A) to (D) are representative of more than three independent experiments.

inhibitor L685,458. This inhibitor neither increased the relative peak height of AICDϵ51 nor reduced that of AICDϵ49/AICDϵ48, suggesting that AICDϵ51 is not a degradation product of AICDϵ49/AICDϵ48 but rather is generated directly by PS/γ-secretase.

These results indicated that there is a striking change in the precision of ϵ-cleavage upon inhibition of endocytosis. We therefore examined whether there is also a parallel remarkable change in the precision of γ-cleavage. We chose IP-MS analysis in order to observe all of the de novo Aβ species. In clear contrast to the analysis of AICD (Figure 2C), IP-MS analysis did not reveal drastic differences in the profiles of de novo Aβ species (i.e., Aβ37, Aβ38, Aβ39, Aβ40, and Aβ42) between reactions using CMF from control cells (Figure 2F, left panel) and cells expressing Dyn-1 K44A (Figure 2F, right panel). Also, very similar results were observed upon inhibition of endocytosis by bafilomycin A1 (Figure 2C in Supporting Information). Immunoprecipitation/immunoblotting analysis for detecting Aβ species revealed a significant decrease upon expression of Dyn-1 K44A (Figure 2G). Thus, in parallel to AICD, we detected a decrease in the level of de novo Aβ levels in the presence of Dyn-1 K44A expression. These results indicated a concomitant decrease in both ϵ- and γ-cleavage efficiencies by PS/γ-secretase upon inhibition of endocytosis.

The Precision of ϵ-Cleavage in the PM-Rich Fractions Is Distinct from That in the Endosome-Rich Fractions. Our cell-free γ-secretase assay revealed that inhibition of endocytosis by expression of the Dyn-1 K44A mutant causes a drastic change in the precision of ϵ-cleavage by PS/γ-secretase but does not concurrently cause such a change in the precision of γ-cleavage. This prompted us to investigate whether there are differences in the precision of ϵ-cleavage on the PM and endosomes. Using CMFs from K293 and HeLa cells, we performed cell-free γ-secretase assays and examined the mass spectra of the generated AICD. As described above (Figures 1D and 2C), in unstimulated K293 and HeLa cells, the relative amounts of ϵ49 and ϵ51 produced are different, indicating that the precision of cleavage at the ϵ-site is distinct in the two cell lines (Figure 3A).

We next examined the production of AICD species in PM- and endosome-rich fractions isolated by iodixanol density gradient centrifugation from CMF prepared from K293 cells expressing βAPP sw. Na−K ATPase, a marker of PM, was detected primarily in the lightest fraction (fraction 1; Figure 3B, first panel), whereas the early endosome markers early endosome antigen 1 (Figure 3B, second panel) and matured nicastrin (Figure 3B, third panel) were detected together in higher density fractions (fractions 4 and 5). GM130, a marker of Golgi, was found mainly in fractions 3 and 7 (Figure 3B, fourth panel). These results suggest that fractions 1 and 5 are the PM- and endosome-rich fractions, respectively. When these fractions were employed in the cell-free γ-secretase assay, we found that the peak height of AICDϵ51 relative to that of AICDϵ49 was larger in the endosome-rich fraction than in the PM-rich fraction (Figure 3C). In contrast, the peak height of AICDϵ49 relative to that of AICDϵ51 was higher in the PM-rich fraction than the endosome-rich fraction (Figure 3C). Similarly, using membrane fractions from HeLa cells, we found that AICDϵ49 was the dominant product in PM-rich fractions, whereas AICDϵ51 was the main product in endosome-rich fractions. These results indicate that the precision of ϵ-cleavage differs on PM and endosomes. Specifically, cleavage at ϵ49, which lies deeper inside the transmembrane domain, tends to occur more on PM than endosomes, whereas the opposite is true for cleavage at ϵ51, which lies closer to the cytosolic side and the interface between transmembrane and intracellular domains.

The Precision of ϵ-Cleavage Is Affected by pH. Our results show that the precision of cleavage at the ϵ-site changes drastically upon inhibition of endocytosis and is affected by the subcellular location. The process of cleavage by PS/γ-secretase may therefore change according to the surrounding conditions. For this reason, we examined whether changing the pH during the cell-free γ-secretase assay affects the level and precision of ϵ- and γ-cleavage. IP-MS showed that, when

Table 1: Amino Acid Sequences of AICDϵ49 and AICDϵ51 Species

MW (obsd)	species	sequence	MW (calcd)
5911	AICDϵ49	V^{646}MLKKKQYTSIHHGVVEVDAAVTPEERHLSKMQQNGYENPTYKFFEQMQN^{695}	5910.7
5680	AICDϵ51	L^{648} KKKQYTSIHHGVVEVDAAVTPEERHLSKMQQNGYENPTYKFFEQMQN^{695}	5680.4

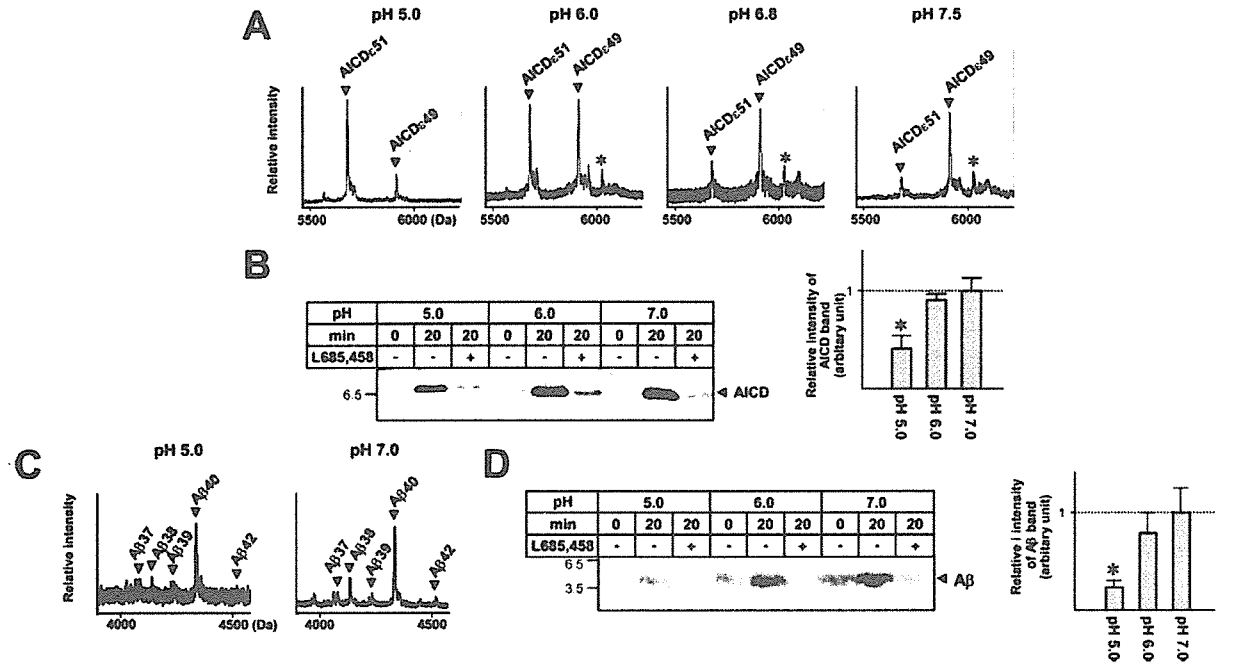

FIGURE 4: Effects of pH on ϵ- and γ-cleavage. (A) Mass spectra of AICD generated in the cell-free assay at pHs between 7.5 and 5.0. CMFs from βAPP sw-expressing K293 cells were resuspended in reaction buffer at the indicated pH. Asterisks indicate AICDϵ48 species. (B) The level of AICDs generated at various pHs. The cell-free incubation was performed in the presence of either L685,458 or vehicle alone (DMSO) (left panel). The asterisk indicates that the intensity of the AICD band at pH 5.0 was statistically lower than those at pH 6.0 and 7.0 ($P < 0.01$ by Student's *t*-test). (C) Mass spectra of Aβ generated in the cell-free assay at pH 5.0 and 7.0. (D) The level of Aβ generated at various pHs and in the presence of L685,458 or vehicle control (DMSO). The asterisk indicates statistical significance ($P < 0.01$ by Student's *t*-test). In (A) and (C) and the left panels of (B) and (D), the results are representative of more than three independent experiments. In the right panels of (B) and (D), the results indicate the means ± standard deviations from at least triplicate determinations.

we changed the buffer pH from 7.5 to 5.0, the relative cleavage efficiency at the ϵ49 and ϵ51 sites changed (Figure 4A). The more acidic the pH, the higher the AICDϵ51 peak became, demonstrating that the pH affects cleavage at the ϵ-site. Immunoblotting also showed that lowering the pH to 5.0 decreased the amount of AICD produced, indicating a reduction in the total amount of cleavage at the ϵ-site (Figure 4B). De novo AICD production was almost completely suppressed by an inhibitor of PS-dependent γ-secretase (L685,458) at various pHs. Therefore, the AICD production that we observed was mostly due to proteolysis by PS-dependent γ-secretase (Figure 4B). These results indicate that alteration of the pH affects both the precision and the level of ϵ-site cleavage. We also studied the effect of pH on the precision and amount of γ-site cleavage. As shown in Figure 4C, we could not detect any ϵ-cleavage-like changes in the precision of γ-cleavage. Also, lowering the pH to 5.0 caused a reduction in the total amount of de novo Aβ production (Figure 4D). Therefore, lowering the pH reduced the level of cleavage at both the γ- and ϵ-sites. Collectively, these results show that the pH in the cell-free assay affects the precision of cleavage at the ϵ-site.

DISCUSSION

In this study, we investigated intramembrane proteolysis of βAPP and demonstrated dynamic changes in the precision of cleavage by the PS/γ-secretase. Using a cell-free γ-secretase assay, we showed that the precision of ϵ-site cleavage changes depending on the subcellular location and pH. These results suggest that the precision of cleavage by the PS/γ-secretase complex can be regulated physiologically.

Inhibition of endocytosis also induced a change in the precision of ϵ-cleavage, suggesting that the function of PS/γ-secretase is related to endocytosis. The precision of ϵ-cleavage on PM and endosomes differs, demonstrating that the function of PS/γ-secretase may be heterogeneous in cells. It is unlikely that the change in precision of ϵ-cleavage observed in this study is due to differences in the thickness of PM and endosome membranes because very similar changes were caused by altering the pH in the cell-free assay. Moreover, our results suggest that the precision of ϵ-cleavage is more dynamic than that of γ-cleavage. Therefore, our results can be explained by (i) additional physiological factors that interact with the active PS/γ-secretase complex or (ii) altered substrate recognition/access at different pH conditions that exist at the plasma membrane and endosomes.

Because the PS/γ-secretase complex mediates both γ- and ϵ-cleavages in the transmembrane domain of βAPP (*2*), one might predict that the processes of γ- and ϵ-cleavage would behave the same. Previous results have shown, however, that the effects of PS mutations on the relative levels of γ42 and

ϵ-site cleavages do not always correlate (*17*). Furthermore, in the current study, we showed that the precision of ϵ- and γ-site cleavages on PM and endosomes did not change in parallel. Our results support the hypothesis that the ϵ-cleavage process is distinct from that of the γ-cleavage, although both occur on the same transmembrane domain and are mediated by the same PS-dependent γ-secretases.

Recent reports have described the existence of several long Aβ species that are thought to be membrane-bound remnants from ϵ-cleavage of CTF stubs (*35*−*37*). Also, it has been reported that there is an association between the cleavages at ϵ51 and at γ42, which are types of ϵ- and γ-site cleavages, respectively (*16*). These findings indicate that there is a time-dependent relationship between γ- and ϵ-cleavages, namely, that γ-cleavage follows ϵ-cleavage (*36*, *37*). If this is generally true, de novo AICD and Aβ is generated from distinct substrates in our cell-free assay; in other words, AICDs is generated from CTF stubs of βAPP, whereas Aβ must be generated from long and membrane-bound Aβ. Otherwise, our results suggest that the process determining the precision of ϵ-cleavage is distinct from that for the γ-cleavage. Thus, it appears that the time-dependent association between γ- and ϵ-cleavages either is not dominant but rather simply reflects the rate of each cleavage under physiological conditions.

In our cell-free assay, conditions mimicking physiological cell functions (i.e., changes in subcellular location, endocytosis, and pH) affected the efficiency of cleavage at ϵ49 and ϵ51; however, we could not find any consistent correlations between relative peak heights of AICDϵ48 and those of AICDϵ49 or AICDϵ51, even though AICDϵ48 was one of the major species.

In summary, we demonstrate here that the precision of ϵ-cleavage of βAPP changes depending on endocytotic function. In future studies, we will examine whether similar changes in the precision of PS-mediated cleavage in the TM-C also occur for other substrates, such as Notch-1.

ACKNOWLEDGMENT

We thank Drs. Harald Steiner, Masaki Nishimura, Maho Morishima-Kawashima, and Yasuo Ihara for critically reading the manuscript. We also thank Drs. Sandra L. Schmid and Takeshi Baba for providing Dyn-1 K44A-expressing HeLa cells.

SUPPORTING INFORMATION AVAILABLE

Four figures indicating that (i) inhibition of endocytosis by bafilomycin A1 treatment caused a drastic change of ϵ-cleavage precision, (ii) the relative ratio of the AICDϵ49 peak height to that of AICDϵ51 semiquantitatively correlated with the relative amount of each AICD species, and (iii) wt βAPP as well as βAPP sw caused the drastic change in the precision of ϵ-cleavage. This material is available free of charge via the Internet at http://pubs.acs.org.

REFERENCES

1. Selkoe, D., and Kopan, R. (2003) Notch and presenilin: regulated intramembrane proteolysis links development and degeneration, *Annu. Rev. Neurosci. 26*, 565−597.
2. Haass, C. (2004) Take five-BACE and the gamma-secretase quartet conduct Alzheimer's amyloid beta-peptide generation, *EMBO J. 23*, 483−488.
3. Okochi, M., Steiner, H., Fukumori, A., Tanii, H., Tomita, T., Tanaka, T., Iwatsubo, T., Kudo, T., Takeda, M., and Haass, C. (2002) Presenilins mediate a dual intramembranous gamma-secretase cleavage of Notch-1, *EMBO J. 21*, 5408−5416.
4. Lammich, S., Okochi, M., Takeda, M., Kaether, C., Capell, A., Zimmer, A. K., Edbauer, D., Walter, J., Steiner, H., and Haass, C. (2002) Presenilin-dependent intramembrane proteolysis of CD44 leads to the liberation of its intracellular domain and the secretion of an Abeta-like peptide, *J. Biol. Chem. 277*, 44754−44759.
5. Okochi, M., Fukumori, A., Jiang, J., Itoh, N., Kimura, R., Steiner, H., Haass, C., Tagami, S., and Takeda, M. (2006) Secretion of the Notch-1 Abeta-like peptide during Notch signaling, *J. Biol. Chem.* (in press).
6. Sastre, M., Steiner, H., Fuchs, K., Capell, A., Multhaup, G., Condron, M. M., Teplow, D. B., and Haass, C. (2001) Presenilin-dependent gamma-secretase processing of beta-amyloid precursor protein at a site corresponding to the S3 cleavage of Notch, *EMBO Rep. 2*, 835−841.
7. Chen, F., Gu, Y., Hasegawa, H., Ruan, X., Arawaka, S., Fraser, P., Westaway, D., Mount, H., and St George-Hyslop, P. (2002) Presenilin 1 mutations activate gamma 42-secretase but reciprocally inhibit epsilon-secretase cleavage of amyloid precursor protein (APP) and S3-cleavage of notch, *J. Biol. Chem. 277*, 36521−36526.
8. Yu, C., Kim, S. H., Ikeuchi, T., Xu, H., Gasparini, L., Wang, R., and Sisodia, S. S. (2001) Characterization of a presenilin-mediated amyloid precursor protein carboxyl-terminal fragment gamma. Evidence for distinct mechanisms involved in gamma-secretase processing of the APP and Notch1 transmembrane domains, *J. Biol. Chem. 276*, 43756−43760.
9. Gu, Y., Misonou, H., Sato, T., Dohmae, N., Takio, K., and Ihara, Y. (2001) Distinct intramembrane cleavage of the beta-amyloid precursor protein family resembling gamma-secretase-like cleavage of Notch, *J. Biol. Chem. 276*, 35235−35238.
10. Weidemann, A., Eggert, S., Reinhard, F. B., Vogel, M., Paliga, K., Baier, G., Masters, C. L., Beyreuther, K., and Evin, G. (2002) A novel epsilon-cleavage within the transmembrane domain of the Alzheimer amyloid precursor protein demonstrates homology with Notch processing, *Biochemistry 41*, 2825−2835.
11. Selkoe, D. J. (2001) Alzheimer's disease: genes, proteins, and therapy, *Physiol. Rev. 81*, 741−766.
12. Weggen, S., Eriksen, J. L., Das, P., Sagi, S. A., Wang, R., Pietrzik, C. U., Findlay, K. A., Smith, T. E., Murphy, M. P., Bulter, T., Kang, D. E., Marquez-Sterling, N., Golde, T. E., and Koo, E. H. (2001) A subset of NSAIDs lower amyloidogenic Abeta42 independently of cyclooxygenase activity, *Nature 414*, 212−216.
13. Kukar, T., Murphy, M. P., Eriksen, J. L., Sagi, S. A., Weggen, S., Smith, T. E., Ladd, T., Khan, M. A., Kache, R., Beard, J., Dodson, M., Merit, S., Ozols, V. V., Anastasiadis, P. Z., Das, P., Fauq, A., Koo, E. H., and Golde, T. E. (2005) Diverse compounds mimic Alzheimer disease-causing mutations by augmenting Abeta42 production, *Nat. Med. 11*, 545−550.
14. Lazarov, O., Robinson, J., Tang, Y. P., Hairston, I. S., Korade-Mirnics, Z., Lee, V. M., Hersh, L. B., Sapolsky, R. M., Mirnics, K., and Sisodia, S. S. (2005) Environmental enrichment reduces Abeta levels and amyloid deposition in transgenic mice, *Cell 120*, 701−713.
15. Sato, T., Dohmae, N., Qi, Y., Kakuda, N., Misonou, H., Mitsumori, R., Maruyama, H., Koo, E. H., Haass, C., Takio, K., Morishima-Kawashima, M., Ishiura, S., and Ihara, Y. (2003) Potential link between amyloid beta-protein 42 and C-terminal fragment gamma 49−99 of beta-amyloid precursor protein, *J. Biol. Chem. 278*, 24294−24301.
16. Funamoto, S., Morishima-Kawashima, M., Tanimura, Y., Hirotani, N., Saido, T. C., and Ihara, Y. (2004) Truncated carboxyl-terminal fragments of beta-amyloid precursor protein are processed to amyloid beta-proteins 40 and 42, *Biochemistry 43*, 13532−13540.
17. Moehlmann, T., Winkler, E., Xia, X., Edbauer, D., Murrell, J., Capell, A., Kaether, C., Zheng, H., Ghetti, B., Haass, C., and Steiner, H. (2002) Presenilin-1 mutations of leucine 166 equally affect the generation of the Notch and APP intracellular domains independent of their effect on Abeta 42 production, *Proc. Natl. Acad. Sci. U.S.A. 99*, 8025−8030.
18. Iwatsubo, T. (2004) The gamma-secretase complex: machinery for intramembrane proteolysis, *Curr. Opin. Neurobiol. 14*, 379−383.
19. Yu, G., Nishimura, M., Arawaka, S., Levitan, D., Zhang, L., Tandon, A., Song, Y. Q., Rogaeva, E., Chen, F., Kawarai, T.,

Supala, A., Levesque, L., Yu, H., Yang, D. S., Holmes, E., Milman, P., Liang, Y., Zhang, D. M., Xu, D. H., Sato, C., Rogaev, E., Smith, M., Janus, C., Zhang, Y., Aebersold, R., Farrer, L. S., Sorbi, S., Bruni, A., Fraser, P., and St. George-Hyslop, P. (2000) Nicastrin modulates presenilin-mediated notch/glp-1 signal transduction and betaAPP processing, *Nature 407*, 48−54.

20. Francis, R., McGrath, G., Zhang, J., Ruddy, D. A., Sym, M., Apfeld, J., Nicoll, M., Maxwell, M., Hai, B., Ellis, M. C., Parks, A. L., Xu, W., Li, J., Gurney, M., Myers, R. L., Himes, C. S., Hiebsch, R., Ruble, C., Nye, J. S., and Curtis, D. (2002) aph-1 and pen-2 are required for Notch pathway signaling, gamma-secretase cleavage of betaAPP, and presenilin protein accumulation, *Dev. Cell 3*, 85−97.
21. Wilson, C. A., Doms, R. W., Zheng, H., and Lee, V. M. (2002) Presenilins are not required for A beta 42 production in the early secretory pathway, *Nat. Neurosci. 5*, 849−855.
22. Lai, M. T., Crouthamel, M. C., DiMuzio, J., Pietrak, B. L., Donoviel, D. B., Bernstein, A., Gardell, S. J., Li, Y. M., and Hazuda, D. (2006) A presenilin-independent aspartyl protease prefers the gamma-42 site cleavage, *J. Neurochem. 96*, 118−125.
23. Okochi, M., Ishii, K., Usami, M., Sahara, N., Kametani, F., Tanaka, K., Fraser, P. E., Ikeda, M., Saunders, A. M., Hendriks, L., Shoji, S. I., Nee, L. E., Martin, J. J., Van Broeckhoven, C., St. George-Hyslop, P. H., Roses, A. D., and Mori, H. (1997) Proteolytic processing of presenilin-1 (PS-1) is not associated with Alzheimer's disease with or without PS-1 mutations, *FEBS Lett. 418*, 162−166.
24. Okochi, M., Eimer, S., Bottcher, A., Baumeister, R., Romig, H., Walter, J., Capell, A., Steiner, H., and Haass, C. (2000) A loss of function mutant of the presenilin homologue SEL-12 undergoes aberrant endoproteolysis in *Caenorhabditis elegans* and increases abeta 42 generation in human cells, *J. Biol. Chem. 275*, 40925−40932.
25. Steiner, H., Romig, H., Pesold, B., Philipp, U., Baader, M., Citron, M., Loetscher, H., Jacobsen, H., and Haass, C. (1999) Amyloidogenic function of the Alzheimer's disease-associated presenilin 1 in the absence of endoproteolysis, *Biochemistry 38*, 14600−14605.
26. Damke, H., Baba, T., Warnock, D. E., and Schmid, S. L. (1994) Induction of mutant dynamin specifically blocks endocytic coated vesicle formation, *J. Cell Biol. 127*, 915−934.
27. Mizutani, T., Taniguchi, Y., Aoki, T., Hashimoto, N., and Honjo, T. (2001) Conservation of the biochemical mechanisms of signal transduction among mammalian Notch family members, *Proc. Natl. Acad. Sci. U.S.A. 98*, 9026−9031.
28. Pinnix, I., Musunuru, U., Tun, H., Sridharan, A., Golde, T., Eckman, C., Ziani-Cherif, C., Onstead, L., and Sambamurti, K. (2001) A novel gamma-secretase assay based on detection of the putative C-terminal fragment-gamma of amyloid beta protein precursor, *J. Biol. Chem. 276*, 481−487.
29. McLendon, C., Xin, T., Ziani-Cherif, C., Murphy, M. P., Findlay, K. A., Lewis, P. A., Pinnix, I., Sambamurti, K., Wang, R., Fauq, A., and Golde, T. E. (2000) Cell-free assays for gamma-secretase activity, *FASEB J. 14*, 2383−2386.
30. Okochi, M., Walter, J., Koyama, A., Nakajo, S., Baba, M., Iwatsubo, T., Meijer, L., Kahle, P. J., and Haass, C. (2000) Constitutive phosphorylation of the Parkinson's disease associated alpha-synuclein, *J. Biol. Chem. 275*, 390−397.
31. Chyung, J. H., and Selkoe, D. J. (2003) Inhibition of receptor-mediated endocytosis demonstrates generation of amyloid beta-protein at the cell surface, *J. Biol. Chem. 278*, 51035−51043.
32. Wolfe, M. S., Xia, W., Ostaszewski, B. L., Diehl, T. S., Kimberly, W. T., and Selkoe, D. J. (1999) Two transmembrane aspartates in presenilin-1 required for presenilin endoproteolysis and gamma-secretase activity, *Nature 398*, 513−517.
33. Kimberly, W. T., and Wolfe, M. S. (2003) Identity and function of gamma-secretase, *J. Neurosci. Res. 74*, 353−360.
34. Stevens, T. H., and Forgac, M. (1997) Structure, function and regulation of the vacuolar (H+)-ATPase, *Annu. Rev. Cell Dev. Biol. 13*, 779−808.
35. Zhao, G., Mao, G., Tan, J., Dong, Y., Cui, M. Z., Kim, S. H., and Xu, X. (2004) Identification of a new presenilin-dependent zeta-cleavage site within the transmembrane domain of amyloid precursor protein, *J. Biol. Chem. 279*, 50647−50650.
36. Qi-Takahara, Y., Morishima-Kawashima, M., Tanimura, Y., Dolios, G., Hirotani, N., Horikoshi, Y., Kametani, F., Maeda, M., Saido, T. C., Wang, R., and Ihara, Y. (2005) Longer forms of amyloid beta protein: implications for the mechanism of intramembrane cleavage by gamma-secretase, *J. Neurosci. 25*, 436−445.
37. Zhao, G., Cui, M. Z., Mao, G., Dong, Y., Tan, J., Sun, L., and Xu, X. (2005) gamma-Cleavage is dependent on zeta-cleavage during the proteolytic processing of amyloid precursor protein within its transmembrane domain, *J. Biol. Chem. 280*, 37689−37697.

BI052412W